


1-1-2016

Investigation Of Mutations In Nuclear Genes That Affect The Atp Synthase

Russell Dsouza
Wayne State University,

Follow this and additional works at: https://digitalcommons.wayne.edu/oa_dissertations

 Part of the [Biochemistry Commons](#), and the [Molecular Biology Commons](#)

Recommended Citation

Dsouza, Russell, "Investigation Of Mutations In Nuclear Genes That Affect The Atp Synthase" (2016). *Wayne State University Dissertations*. 1526.
https://digitalcommons.wayne.edu/oa_dissertations/1526

This Open Access Dissertation is brought to you for free and open access by DigitalCommons@WayneState. It has been accepted for inclusion in Wayne State University Dissertations by an authorized administrator of DigitalCommons@WayneState.

**INVESTIGATION OF MUTATIONS IN NUCLEAR GENES
THAT AFFECT THE ATP
SYNTHASE**

by

RUSSELL L. D'SOUZA

DISSERTATION

Submitted to the Graduate School

of Wayne State University,

Detroit, Michigan

in partial fulfillment of the requirements

for the degree of

DOCTOR OF PHILOSOPHY

2016

MAJOR: BIOCHEMISTRY & MOLECULAR
BIOLOGY

Approved By:

Advisor

Date

**© COPYRIGHT BY
RUSSELL L. D'SOUZA
2016
All Rights Reserved**

DEDICATION

I dedicate my dissertation work to my family. My deepest gratitude to my parents, Raymond and Emma D'Souza, whose constant support has helped me pursue my dreams. My brother Reuben, who has always been there by my side.

I also dedicate this thesis to my wife, Jayshree Bhakta, who has always been there for me during the difficult times at graduate school. I will always appreciate all that she's done for me and for all the encouragement. She's been the best cheerleader in my life.

Finally, a special thanks to my best friend Joe D. Klavitter and his wife Jessica, for all the help and the much needed love. You guys truly are the best and thank you for being there for me.

ACKNOWLEDGEMENTS

I want to take this opportunity to thank several people without whom this thesis would have never been written and this journey never completed.

I am highly indebted to my Ph.D. supervisor, Dr. Sharon Ackerman, for accepting me in the laboratory as a graduate student and for introducing me to the world of mitochondrial biology, a field that I was not too familiar with. It was because of her scientific guidance, cheerful enthusiasm, and her ability to ask the right scientific questions that I was able to complete my doctoral studies in a respectable manner. The one virtue that I would want to emulate from Dr. Ackerman is to pay attention to detail, whether it be scientific experiments or other aspects of my graduate training. All of the knowledge that I possess with regards to mitochondrial biology, I owe it to her. She will continue to inspire me in many ways.

I wish to express gratitude to my dissertation committee members, Dr. David Evans, Dr. Domenico Gatti, and Dr. Miriam Greenberg. Their thoughts and suggestions at the various committee meetings has been highly invaluable and has nurtured me to be a better graduate student. I cannot thank them enough and will always be indebted to them.

I would also like to thank everybody at the Department of Biochemistry and Molecular Biology, for accepting me into their graduate program and for their constant help and support. My deepest gratitude to the departmental graduate committee for helping me out in all of the difficult situations. A big thank you to the administrative staff, without whom the graduate paperwork would have never been in order.

Finally, I would like to thank the IBS, my family and the many friends that have been with me throughout this incredible journey.

TABLE OF CONTENTS

DEDICATION.....	ii
ACKNOWLEDGEMENTS	iii
LIST OF TABLES	vi
LIST OF FIGURES	vii
CHAPTER 1: INTRODUCTION.....	1
1.1 General Introduction	1
1.2 Advantages of the yeast model to study mitochondrial energy metabolism	2
1.3 ATP Synthase structure.....	5
1.4 Assembly of the mitochondrial ATP synthase.....	8
1.5 Mechanism of ATP synthesis	10
1.6 Human pathologies linked to the mitochondrial ATP synthase	13
CHAPTER 2: MATERIALS AND METHODS	18
Cells and Media.	18
Preparation of yeast mitochondria	18
ATPase assays.....	19
Extraction of F₁F_o from mitochondria.....	20
Step sucrose centrifugation analysis of F₁-ATPase subunits.....	20
Linear sucrose centrifugation analysis of soluble F₁F_o.	21
Western blotting analysis.....	22
Yeast transformations.....	23
Lactate dehydrogenase (LDH) assay.	24

CHAPTER 3: CHARACTERIZATION OF MUTATIONS IN NUCLEAR GENES ENCODING THE α-SUBUNIT OR β-SUBUNIT OF YEAST MITOCHONDRIAL F₁	26
Summary	26
Results	29
Discussion.....	44
CHAPTER 4: ACCOUNTING FOR POLYMORPHISMS IN THE HUMAN <i>ATP12</i> GENE (<i>ATPAF2</i>) THAT AFFECTS F₁ BIOGENESIS.....	55
Summary	55
Results and discussion.....	56
CHAPTER 5: THE N-TERMINAL DOMAINS OF ATP11P.....	60
Summary	60
Results and Discussion	62
CHAPTER 6: SCOPE OF THE STUDY AND LIMITATIONS	66
REFERENCES.....	69
ABSTRACT.....	82
AUTOBIOGRAPHICAL STATEMENT	84

LIST OF TABLES

Table 1. Subunit composition of human, yeast, and <i>Escherichia coli</i> ATP synthase.....	6
Table 2. ATPase activities of <i>atp1</i> mutants.	30
Table 3. ATPase activities of <i>atp2</i> mutants.	31
Table 4. Mutations in the α subunit of yeast F ₁	44
Table 5. Mutations in the β subunit of yeast F ₁	45
Table 6. ATPase activities of yeast producing plasmid-borne Atpaf2p.	57
Table 7. ATPase activities of yeast producing plasmid-borne Atp11p variants.....	63

LIST OF FIGURES

Figure 1. The chemiosmotic model	2
Figure 2. Cartoons of the yeast mitochondrial ATP synthase	5
Figure 3. Model of ATP synthase assembly in yeast mitochondria	9
Figure 4. The mechanism of ATP synthesis	12
Figure 5A. Mutant genes cloned and sequences from <i>atp1</i> and <i>atp2</i> yeast strains belonging to complementation groups (G50, G1) of respiratory-deficient nuclear mutants	27
Figure 5B. Oligomycin distinguishes F_1 that is coupled F_0 from uncoupled F_1	29
Figure 6. Western blots of F_1 α and β subunits in Triton X-100 extracted mitochondria from <i>atp1</i> mutants.....	33
Figure 7. Western blots of F_1 α and β subunits in Triton X-100 extracted mitochondria from <i>atp2</i> mutants.....	34
Figure 8. Western blots of step sucrose gradient fractions	36
Figure 9. Sedimentation analysis of the F_1 protein in Triton X-100 extracts of mitochondria from the wild type D273	37
Figure 10. Sedimentation analysis of the F_1 protein in Triton X-100 extracts of mitochondria from <i>atp2</i> mutant E323	38
Figure 11. Sedimentation analysis of the F_1 protein in Triton X-100 extracts of mitochondria from <i>atp2</i> mutant E892	40
Figure 12. Sedimentation analysis of the F_1 protein in Triton X-100 extracts of mitochondria from <i>atp1</i> mutant E793	41
Figure 13. Sedimentation analysis of the F_1 protein in Triton X-100 extracts of mitochondria from additional <i>atp1</i> mutants	41
Figure 14. Sedimentation analysis of the F_1 protein in Triton X-100 extracts of mitochondria from <i>atp2</i> mutant N15.....	42
Figure 15. Yeast F_1 α_C subunit.....	44
Figure 16. Yeast F_1 β_D subunit	45

Figure 17. <i>atp1</i> mutations correlated with Class 1 assembly defects	47
Figure 18. Location of the adenine nucleotide binding sites in F ₁	50
Figure 19. Model of the <i>atp2</i> mutation G323D.....	51
Figure 20. Structure models showing the relative positions of the G227D and D469N mutations D469N mutations in the yeast F ₁ β subunit	53
Figure 21. Western analysis showing solubilization of the F ₁ F ₀ from yeast mitochondria...	57
Figure 22. Step sucrose density gradients of plasmid-borne Atp12p variants	58
Figure 23. Structure and domains of Atp11p	60
Figure 24. Western analysis showing F ₁ F ₀ extraction from yeast producing Atp11p from plasmids	64
Figure 25. Protein blots of mitochondria from yeast transformants that produce Atp11p proteins from plasmids.....	64

CHAPTER 1: INTRODUCTION

1.1 General Introduction

Most of life's energy consuming processes are fueled by adenosine-5'-triphosphate (ATP). The majority of ATP synthesis takes place inside mitochondria during aerobic respiration by the process known as oxidative phosphorylation (OxPhos) in which redox energy is used to create a bond between ADP and inorganic phosphate (Pi). Respiratory substrates are oxidized by the components of an electron transport chain (ETC) located in the mitochondrial inner membrane that transfer the reducing equivalents to molecular oxygen (O₂) forming water. There are four different respiratory substrates (NADH, succinate, fatty-acyl CoA, glycerol-3-phosphate) and separate dehydrogenase enzymes for each. All four dehydrogenases transfer reducing equivalents from the respective substrate to a common acceptor, ubiquinone (Coenzyme Q, "Q"), which gets reduced to ubiquinol (QH₂). Electrons are then transferred along a linear path to O₂ through redox centers in the ubiquinol:cytochrome *c* oxidoreductase (*bc₁* complex), cytochrome *c*, and cytochrome *c* oxidase. The redox reactions are exergonic and part of the energy released is utilized by ETC proteins to translocate protons from the matrix compartment to the intermembrane space (IMS). This action creates a transmembrane electrochemical gradient with the IMS more positively charged and acidic relative to the matrix. The pressure to counteract the imposed change in proton distribution constitutes an energy source called the proton motive force (*pmf*). The mitochondrial ATP synthase uses the *pmf* to make ATP (Figure 1, image adapted from "Lehninger Principles of Biochemistry (5E 2008 ISBN 9780716771081) David L. Nelson, Michael M. Cox).

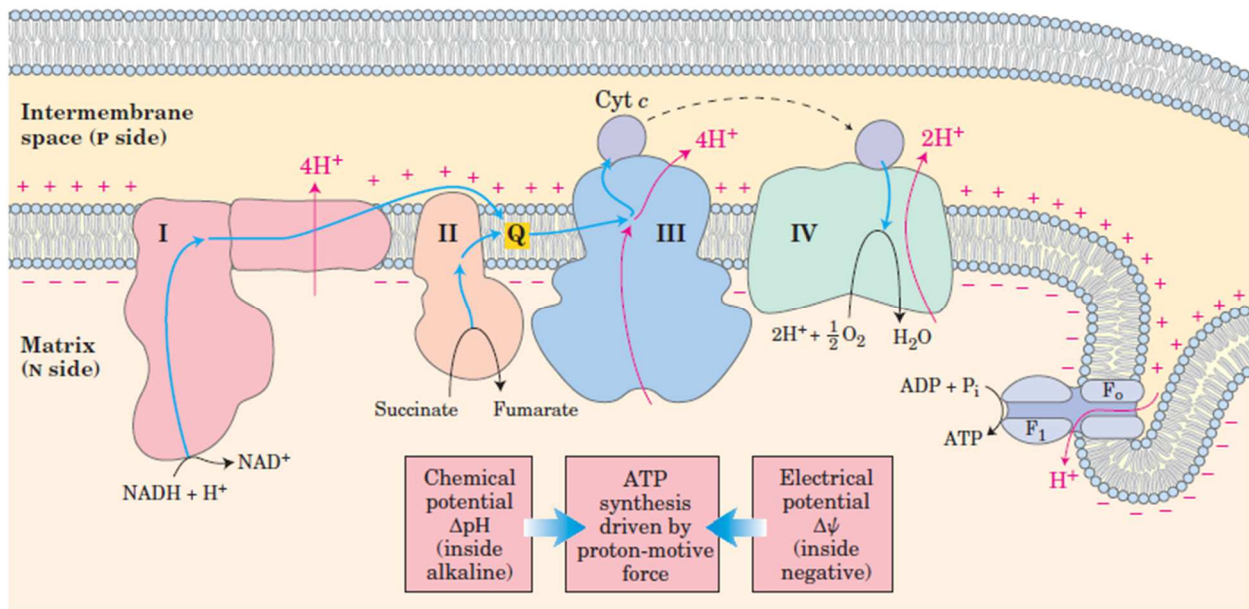


Figure 1. The chemiosmotic model. Electrons from oxidizable substrates pass through a series of electron carriers located in the inner mitochondrial membrane (IM). Electron flow is accompanied by the movement of protons across the membrane to produce a chemical gradient (ΔpH) and an electrical gradient ($\Delta\Psi$). Together, these gradients comprise a proton motive force (pmf) that allows the protons to re-enter the mitochondrial matrix via a polar channel in the F_0 region, and this action provides the energy for ATP synthesis catalyzed by the F_1 .

1.2 Advantages of the yeast model to study mitochondrial energy metabolism

Most of what we know about the mitochondria originates from studies that were conducted in the yeast *Saccharomyces cerevisiae*. *S. cerevisiae* has the ability to survive mutations in the oxidative phosphorylation (OxPhos) system when provided with a fermentable carbon source such as glucose, thus establishing a genetic system for studying mitochondria 60 years ago (1). Studies in *S. cerevisiae* mutant forms (ρ^-/ρ^0) revealed that a non Mendelian genetic element, the ρ factor, is responsible for the control of respiration in yeast, which was found later to be a 16 kB DNA (mt DNA) molecule located in the mitochondrion (2). Due to a smaller size and limited coding genes, it was quickly realized that the majority of the fundamental genes needed for the process of mitochondrial biogenesis must reside within the nuclear DNA (nDNA) and the products transported to the mitochondria. The role of nDNA in

the regulation and expression of mitochondrial genes was confirmed by Alexander Tzagoloff by establishing the existence of > 200 genetically distinct nuclear loci required for the growth of yeast cells on non-fermentable substrates such as glycerol (3). The construction of whole-genome deletion-mutant collections and sequencing of the *S.cerevisiae* genome has led to the identification of 265 previously unknown nuclear genes required for optimal growth using respiration (4). Furthermore, proteomic analysis of highly pure yeast mitochondria using mass spectroscopy has approximately 1000 total protein species in yeast mitochondria (5, 6). Remarkably, on analyzing 14 different mouse tissues, a similar count of mitochondrial proteins was estimated, of which greater than 50% had a homolog in yeast (7). Such observations indicate that the mitochondria of single-celled organisms are complex in nature and are highly similar to the individual cells of higher eukaryotes.

The human mitochondrial genome database (MITOMAP) has identified more than 250 point mutations that are proven or suspected to be pathogenic (<http://www.mitomap.org>). Mutations in genes that encode a mitochondrial protein primarily affect the complexes to which they belong, whereas, mutations in the mitochondrial transfer RNA (mt-tRNA) genes have a pleiotropic effect because they impair the entire process of mitochondrial protein synthesis. Unique characteristics of mitochondrial genomes (8) and technical challenges have significantly hampered genetic experiments with human mtDNA. The mitochondrial genome is susceptible to a rate of mutation that is 10-17 times higher relative the nuclear chromosomes and the prevalence of family or population specific polymorphisms makes it difficult to discern between a neutral mtDNA variant and one that is disease-causing. Also, the mitochondrial genome is polyploid and can accumulate in hundreds or thousands of copies in a single cell. This latter property has particular consequence for studies of mtDNA mutations in human cells, which are

typically heteroplasmic. A further complication has been the dismal failure in developing a practical method to introduce mutagenized mtDNA directly and stably into the mitochondria of a mammalian cell (9).

S. cerevisiae has been invaluable for the investigation of mutations in mtDNA mutations for two reasons. First, since it is unable to stably maintain a heteroplasmic mitochondrial genome it is relatively easy to obtain homoplasmic populations of budding yeast in which all mtDNA molecules carry a mutation of interest (10). Second, it is the only species amenable to targeted genetic manipulation of mtDNA; mutant DNA sequences can be delivered into yeast mitochondria by microprojectile bombardment (biolistic transformation) and subsequently incorporated into mtDNA by the highly active homologous recombination machinery present in the organelle (11). The high level of functional conservation between yeast and human mitochondrial genes legitimizes the yeast model for revealing the molecular mechanisms of pathogenic human mitochondrial gene mutations (10). Progress to date has included the characterization of various mutations in yeast mitochondrial genes encoding the subunits of the OxPhos complexes (12) and the mt-tRNAs (13). Of particular note has been the ability of investigators to recapitulate in yeast and study the effects of the human *ATP6* mutations that cause the mitochondrial myopathies NARP (neuropathy, ataxia, and retinitis pigmentosa) and Leigh syndrome (14). *S. cerevisiae* has also provided efficient means to study mitochondrial diseases that are caused by mutations in the nuclear genome. Since the first report in 1995 of nuclear defect affecting respiratory complex II (succinate dehydrogenase) in sibling patients with Leigh syndrome (15), more than 150 nuclear genes have been linked to mitochondrial diseases, ~70% of which are conserved in yeast (16–18).

1.3 ATP Synthase structure

The structure of the ATP synthase is essentially the same across the bacterial, plant, and animal kingdoms, although there are many more composite subunits in eukaryotes vs prokaryotes (Table 1). The cartoon

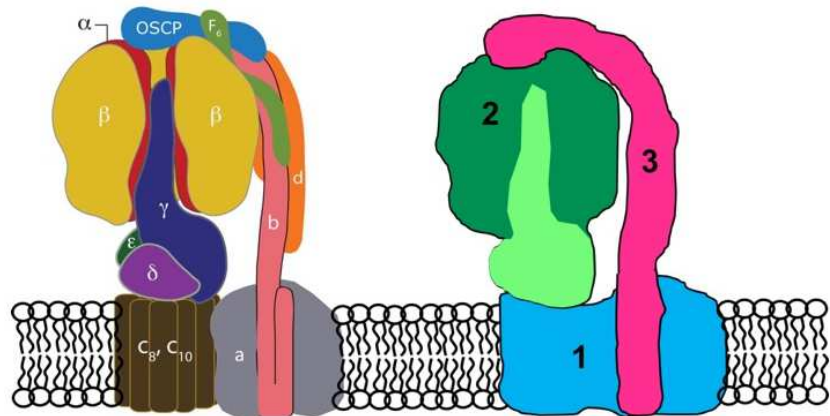


Figure 2. Cartoons of the yeast mitochondrial ATP synthase. The *left-hand* diagram shows the names of the major subunits and the *right-hand* diagram shows the demarcation of three structural domains. See text for details.

drawings of the yeast mitochondrial ATP synthase in Figure 2 depict the general arrangement of the individual subunits (*left*) and the domain architecture of the protein (*right*). Domain 1 (*sky blue*) is hydrophobic and spans the mitochondrial inner membrane. There is an evolutionarily conserved core structure that contains a single *a* subunit in contact with an oligomer of *c* subunits. The *a/c*-ring interface serves as a polar channel that conducts protons across the membrane. Domain 2 (*green*) is hydrophilic and projects into the matrix. This domain can be readily purified from the membrane as a single unit and is named F_1 . F_1 is the catalytic component of the ATP synthase.

Table 1. Subunit composition of human, yeast, and *Escherichia coli* ATP synthase.^a

Subdomain	Stoichiometry	Bacteria	Mitochondria	
		<i>E. coli</i>	<i>S. cerevisiae</i>	<i>H. sapiens</i>
F ₁	3	α	α	α
	3	β	β	β
	1	γ	γ	γ
	1	ε	δ	δ
	1	-	ε	ε
	1	δ	OSCP ^b	OSCP ^b
F ₀	1	<i>a</i>	<i>a</i> (Atp6p)	<i>a</i>
	10-15	<i>c</i>	<i>c</i> (Atp9p)	<i>c</i>
	1-2 ^c	<i>b</i>	<i>b</i> (Atp4p)	<i>b</i>
	1	-	d	d
	1	-	h	F ₆
	1	-	8 (Atp8p)	A6L
	1		f	f
	tbd ^d	-	e	e
	tbd	-	g	g
	1	-	i	-
	1	-	k	-
	Regulators	1		Inh1p
	tbd		Stf1p	
	tbd		Stf2p	

^aThis table is adapted from Rodenberg *et al.* J Inherit Metab Dis (2012) 35:211–225, Table 1.
^bOligomycin-sensitivity conferring protein. The mitochondrial OSCP does not co-purify with solubilized F₁, while its bacterial homolog (δ) does.
^cThe *E. coli* enzyme has two copies of the *b* subunit, while in mitochondria there is one *b*-homolog and subunits d and h/F₆ that fulfill the role the second bacterial *b* subunit.
^dto be determined.

Five different types of F₁ subunits are distributed between two sub-structures: one is spherical with 3α subunits and 3β subunits (*dark green*) and the other is an elongated rod made up of γ, δ, and ε subunits (*light green*). The *left-hand* diagram in Fig. 2 shows that the α subunits (*red*) and the β subunits (*gold*) alternate with each other in the sphere. Each β subunit contains an adenine nucleotide binding site that becomes catalytically active in the assembled enzyme where there is contribution from an adjacent α subunit (19). The rod, which is commonly referred to as the “rotor” (see below), is mostly comprised of the γ subunit, part of which extends up inside the αβ hexamer. The δ and ε subunits associate with γ at the base of the structure, and are necessary

to connect the γ subunit to the c -ring. Domain 3 (*magenta*) is a peripheral stalk that is anchored in the membrane at one end and connects with the $\alpha\beta$ hexamer at the other end. The best characterized proteins of the peripheral stalk are subunits b , d , F6, and OSCP. Domains 1 and 3 constitute what has been historically called the F_0 component of the ATP synthase.

The stoichiometry of the c -ring varies between species with *E. coli* (20, 21) and yeast (22) having a c_{10} oligomer, while the F_0 domains of *Ilyobacter tartaricus* (23), *Chlamydomonas* (24) and spinach chloroplasts (25) have c_{11} , c_{13} and c_{14} multimers, respectively. The c -ring of the cyanobacterium *Spirulina platensis* contains 15 subunits and is the largest known (26). The differences between organisms are interesting because the c -ring stoichiometry determines the number of protons that pass through the a/c -ring channel per ATP synthesized. Every 360° rotation of the c -ring (plus rotor unit) affords 3 ATPs released from the enzyme. Accordingly, in yeast that have a c_{10} -ring, the proton to ATP ratio would be 3.3 (10/3) while in chloroplasts the ratio would be 4.7 (14/3). The significance of the proton to ATP (H^+/ATP) ratio can be explained thermodynamically. Under physiological conditions, the energy required for ATP synthesis is 50 kJ mol^{-1} ($\sim 520 \text{ meV}$). The proton motive force ranges between 120-200 mV, and is equal to the energy released for every proton that re-enters the mitochondrial matrix. Hence, nearly 3 protons must be transferred through the channel in F_0 to generate the 520 meV necessary to make 1 ATP. A consensus has been reached among bioenergetists that there are 10 protons translocated from the matrix to the IMS per NADH oxidized and 6 for either succinate, fattyacyl-CoA, or glycerol-3-P, all of which transfer electrons to ubiquinone *via* redox pathways that generate $FADH_2$ along the way. Assuming these values are universally equivalent, the amount of substrate oxidized per ATP would need to increase in concert with the c -ring stoichiometry to permit, for example, a comparable amount of ATP synthesis in

chloroplasts and in yeast mitochondria. It follows that the efficiency of oxidative energy metabolism correlates inversely with the stoichiometry of the *c*-ring

1.4 Assembly of the mitochondrial ATP synthase

The biogenesis of eukaryotic ATP synthase involves two separate genomes and three sub-cellular compartments. Most of the subunits are nuclear gene products, which are translated in the cytoplasm and imported to destinations in the matrix or the inner membrane of mitochondria. However, 2 or 3 of the most hydrophobic F_0 proteins are encoded by mtDNA and translated inside the organelle; in *S. cerevisiae*, subunits *a*, *c*, and 8 are mitochondrially encoded, while in higher eukaryotes the gene for the *c*-subunit is nuclear. Adding to the complexity of mitochondrial ATP synthase biogenesis is the involvement of “assembly factors” that mediate productive associations among unassembled ATP synthase subunits, and the non-conserved F_0 proteins that foster the dimerization of the enzyme in the membrane. Most of the genes encoding these functions were cloned by complementing respiratory-deficient nuclear mutants of the Tzagoloff *S. cerevisiae* collection (3) (see above), and work over the past 25 years has mapped these functions to discrete steps along the biogenesis pathway for the yeast enzyme (Figure 3)

The soluble F_1 component of the mitochondria, which includes the $\alpha_3\beta_3$ hexamer and the $\gamma\delta\epsilon$ rotor element, is assembled independently from the peripheral stator and the membrane-embedded F_0 subunits. In yeast deficient for either Atp11p or Atp12p, the α and β subunits both accumulate as aggregated proteins (27). Subsequent studies showed evidence of direct protein interactions between Atp11p and the β subunit (28), and between Atp12p and the α subunit (29). Additional insight to the F_1 assembly pathway came from experiments with yeast $\Delta atp1$ and $\Delta atp2$ mutants lacking either the α or β subunit, respectively. Only one of the two types of hexamer proteins is produced in such yeast and when present by itself, the lone β or α subunit is

recovered as insoluble material following fractionation of mitochondria (27). Cumulatively, the data was interpreted to indicate (1) the individual α and β subunits are naturally prone to aggregation, (2) Atp11p protects F₁ β and Atp12p protects F₁ α from aggregation *in vivo*, (3) the level of the assembly factors inside mitochondria is vastly substoichiometric with respect to target protein, which would explain the β subunit aggregates in $\Delta atp1$ (or *vice versa*); there

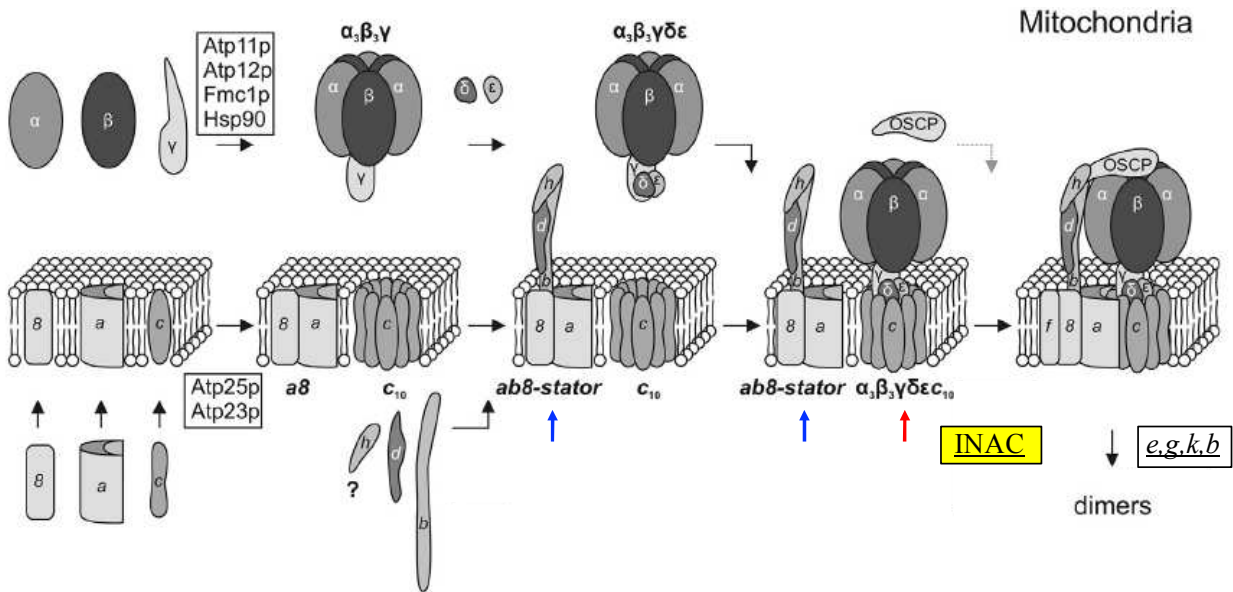


Figure 3. Model of ATP synthase assembly in yeast mitochondria. The cartoon in this figure was adapted from Lesiter *et al*, Assembly of F₁F₀ ATP Synthase, *Biochim Biophys Acta* (2015), Figure 1A.

simply is not enough Atp11p (or Atp12p) to maintain a full complement of the β subunit (or α subunit) in a soluble state (30). In addition to the normal house-keeping functions fulfilled by the Atp11p and Atp12p molecular chaperones, Fmc1p (31) and Hsp90p (32) were identified to be required for yeast F₁ assembly under conditions of heat stress.

Mitochondrial F₀ assembly occurs in stages that are characterized by unique sub-assemblies (33). The *c*-ring forms as a distinct entity that binds the F₁ oligomer before interacting with any other F₀ protein (34) (Fig. 3, *red arrow*). The other two major integral membrane proteins, subunits *a* and δ , form a binary complex that matures into a larger complex

(*blue arrows*) through binding 2 or 3 stator stalk subunits (*b*, *d* and probably *h*). The later steps are coordinated by an entity called the mitochondrial inner membrane assembly complex (INAC, *yellow shading*), which mediates binding in the matrix compartment between F_1 , the membrane-associated stator stalk proteins, and OSCP, and in the membrane between the *a* subunit and *c*-ring to create the proton channel (35). The ramifications of postponing subunit *a* association with the *c*-ring until OSCP can bind and secure F_1 to the membrane domain cannot be overstated. This temporal relationship ensures that the rotor element is engaged when the proton channel is formed and avoids the risk of *pmf* dissipation without ATP generation

The ability of mitochondrial ATP synthase to form dimers (36) is an interesting feature because there have been experimental observations that link this phenomenon to mitochondrial cristae development (36, 37). Work that has included Blue-native gel electrophoresis (38) to separate membrane complexes in samples of digitonin-treated yeast mitochondria has associated three of the non-conserved F_0 subunits of eukaryotes (*e*, *g*, and *k*) (see Table 1) with dimer formation, though none of these proteins are essential for ATP synthase activity (37). There is also a eukaryotic-specific transmembrane domain at the N-terminus of the *b* subunit that has been shown to bind the *g* subunit, which implicates also this protein in dimer formation (39). A structure of the ATP synthase dimer at 3.7 nm resolution has been obtained using electron cryotomography, which reveals a V-like structure with the two monomers separated by an angle of 86° at the long axes (40).

1.5 Mechanism of ATP synthesis

Investigators in the bioenergetics field concur on the point that the ATP synthesis and the ATP hydrolysis reactions catalyzed by the ATP synthase proceed according to the same mechanism, albeit in opposite directions. Most of what is known about this mechanism has

come from studies of the hydrolysis reaction because it is so much easier to measure this activity *in vitro*. The measurements of rate constants in Dr. Harvey Penefsky's laboratory (41, 42) and of the patterns of ^{18}O exchange for substrates and products by Dr. Paul Boyer and colleagues (43) constituted seminal work during the early 1980's that revealed the three catalytic sites of F_1 operate cooperatively during enzyme turnover; the catalytic rate at one CS was shown to be increased by substrate binding to at least one additional CS in the enzyme. This feature was verified a decade later from the first high resolution X-ray structure of mitochondrial F_1 (19) (Figure 4), which showed that the 3 catalytic sites differed in structure and nucleotide occupancy. Moreover, the catalytic sites were located to every other subunit interface around the perimeter of the $\alpha_3\beta_3$ hexamer, with the cavity in the β subunit and critical side-chain contribution from the α subunit. The features of the CS asymmetry are modeled in the cartoons shown in Fig. 4; the TP site has a closed conformation with nucleotide triphosphate bound, the DP site (with bound ADP) is looser in comparison, and the E site is wide open and empty. The γ subunit, which is observed in the center of the $\alpha_3\beta_3$ hexamer, is connected at the other end to the c -ring of F_0 in the assembled F_1F_0

To explain the mechanism of ATP synthesis it is convenient to begin with the hypothetical situation in which there is no respiratory substrate in mitochondria. Under such circumstance the F_1 would likely resemble the cartoon at the top of Fig. 4, in which ATP is trapped in the closed TP site, $\text{ADP} \pm \text{Pi}$ is bound to the DP site, and an empty third site.

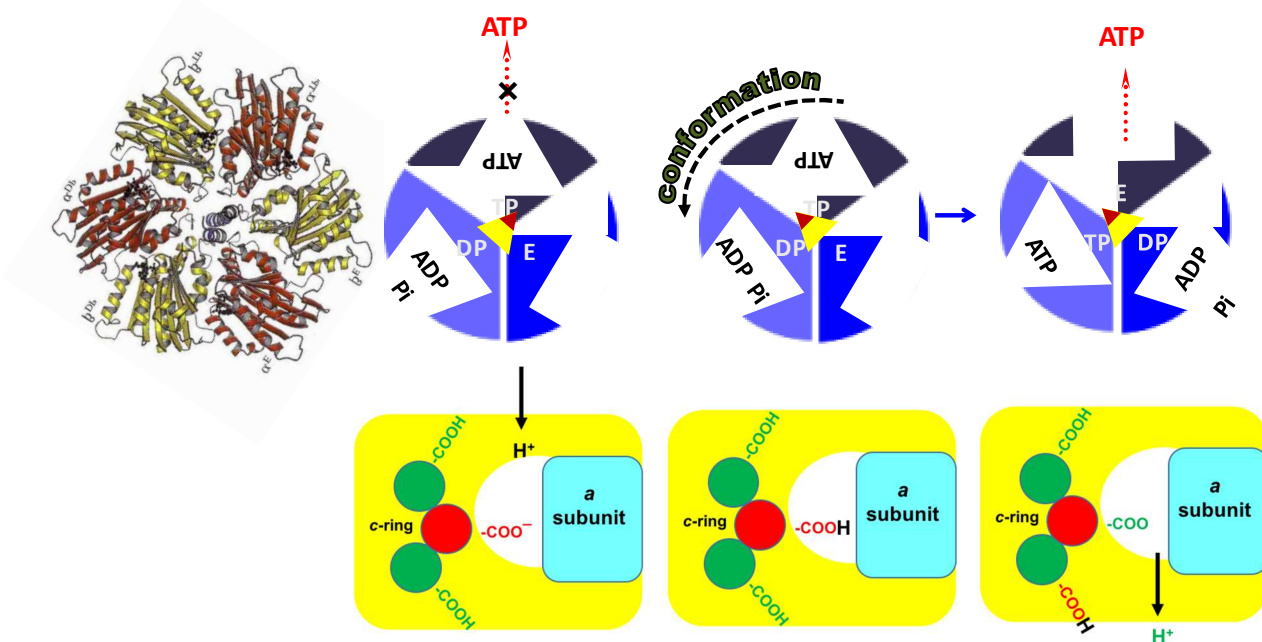


Figure 4. The mechanism of ATP synthesis. *Upper*, Views looking down on the top of the bovine mitochondrial F_1 are shown with side by side images of the 2.8 Å structure model (1BMF.pdb) and a cartoon. The three catalytic subunits are the β_{TP} , β_{DP} , and β_E sites, and the γ subunit is portrayed by the *yellow* triangle with the orientation highlighted *red*. *Lower*, Cartoon view of mitochondrial IM cross-section showing the proton channel (white) at the *a/c*-ring interface. Subunit *c*-carboxylate can be ionized inside the polar channel but must be protonated when exposed to surrounding lipid.

When reducing equivalents are provided, the respiratory chain translocates protons out of the mitochondrial matrix, generating the proton motive force that drives ATP synthesis. In an effort to release the *pmf*, protons flow down the energy gradient from the IMS to the matrix through the *a/c*-ring channel in the membrane (Fig. 4, *lower*). Ion entry protonates the negatively charged carboxyl group of the *c*-subunit exposed to the polar environment in the channel. Neutralization of the charge enables the *c*-ring to rotate such that the newly protonated *c*-subunit moves to the lipid bilayer, the adjacent *c*-subunit moves to the polar channel and loses its proton, which is then transferred to the other side of the membrane. The attached γ subunit rotates with the *c*-ring (see Fig. 4, *upper*, *orientation of triangle*), and this brings about conformational changes at the catalytic sites. The final result is that what was formerly a TP site

releases the bound ATP to become an E site, the DP site locks in the Pi to form a TP site and the E site binds an ADP to form a DP site.

1.6 Human pathologies linked to the mitochondrial ATP synthase

OxPhos deficiency caused by genetic defects in the human ATP synthase (complex V) are much less common compared with those that have been linked to the respiratory proteins of the ETC. According to the diagnostic data that has been collected for human mitochondria, the frequencies at which genetic mutations have been linked to disease are 8% for complex I (NADH:ubiquinone reductase), 5% for complex IV (cytochrome *c* oxidase), 3% for complex III (ubiquinol:cytochrome *c* oxidoreductase), 2% for complex II (succinate:ubiquinone reductase) and 1% for complex V (1%) (44). Mutations in *ATP6* and *ATP8*, encoded by human mtDNA, are the most common sites of genetic lesions linked to complex V deficiency. To date there have been only three nuclear genes (*ATPAF2*, *TMEM70*, *ATP5E*) for which mutations linked to complex V deficiency have been reported. The features of complex V-linked diseases of OxPhos are described briefly in the following sub-sections of this topic.

1.6.1 ATP synthase α mutations: *ATP5A1*

Two missense mutations in the human nuclear gene, *ATP5A1*, were identified in two separate cases. In the first case a mutation was observed that converted a Tyr278Cys in an infant (45). The symptoms of the mutation were similar to severe mitochondrial diseases leading to the death of child at age 3. The patient had a sister with similar symptoms and died at age 15. Both patients had combined respiratory chain deficiency. The effect of the mutation was more severe in the muscle and the liver of the patient with depletion of the mitochondrial DNA. Studies in yeast has revealed that this α subunit mutation uncouples the F₁ ATP synthase. In the second case an Arg286Cys was observed in the α subunit of two siblings (46). The mutation caused

severe cerebral damage leading to death of both siblings within the first few weeks of birth. In addition, damage to the kidney, lungs, and skeletal muscle was also observed. The Arg286Cys mutation caused a dramatic decrease in the ATP production levels as measured by ATP activities. While the father was a heterozygote carrier of the mutation, the mother had another mutation that caused the loss of expression of the gene coding the α subunit. Both patients were heterozygous for the Arg286Cys mutation and did not express any wild-type form of the α subunit. This mutation did not manifest any pleiotropic effects on the mitochondrial DNA or other respiratory chain enzymes.

1.6.2 ATP synthase subunit *a* mutations: *ATP6*

The first and the most frequently reported complex V genetic defects are due to mutations in the mitochondrial encoded *ATP6* gene (47). The most common mutations that affect *ATP6* are m.8993T>G/C, and m.9176T>G/C, and the symptoms of this mutation varies between isolated ataxia, NARP, bilateral striatal necrosis, to Leigh or Leigh-like syndromes (48–50). Also, other clinical mutations have been associated with *ATP6* (www.mitomap.org). The m.8993T>G mutation leads to NARP (<90-95%) or MILS (>95%) depending upon the level of heteroplasmy. The m.8993T>G point mutation leads to the substitution of arginine for leucine at position 156 in the protein. L156 is highly conserved in eukaryotes (51, 52). The mutation has no effect on complex V assembly, but does replace a neutral for a positive charge at the *a/c*-ring ring interface slowing proton translocation through the channel (53). Clinically the symptoms of m.8993T>C are similar to m.8993T>G, but the effects are milder (54, 55). The former leads to the substitution of proline for L156, which in a manner not understood, correlates with a higher production of reactive oxygen species (ROS) that is believed to be the primary cause of pathogenicity (51). ROS is known to be a major player in the pathogenesis of many different

neurological disorders that are related to mitochondrial dysfunctions (56). The m.9176T>G/C is characterized by familial bilateral striatal necrosis (FBSN) and Leigh syndrome (57). These mutations convert L217 to R217 (m.9176T>G) or to P117 (m.9176T>C), which is another *a* subunit residue that is located proximal to the *c*-ring. However, studies in yeast have shown that this mutation blocks, almost completely, the incorporation of the *a* subunit in the ATP synthase and impacts complex V assembly unlike the m.8993T>G/C mutations described above.

1.6.3 ATP Synthase subunit A6L mutation: *ATP8*

A m.8529G>A homoplasmic mutation was observed in the mitochondrial genome of a 16-year old patient, which caused apical hypertrophic cardiomyopathy and neuropathy (58). It overlaps a region between *ATP6* and *A6L*, and leads to a silent change in *ATP6* but introduces a premature stop codon in a conserved region of *A6L*. This mutation led to an assembly defect and decreased ATP production by complex V. The m.8528T>C mutation was observed in four infants from unrelated families who presented with isolated hypertrophic cardiomyopathy and congestive heart failure, leading to multisystem disease (59). m.8528T>C causes the substitution W55R at a highly conserved tryptophan in *A6L*. Another *A6L* mutation, m.8411A>G, was reported in a patient suffering from psychomotor delay, epilepsy, tetraplegia, congenital deafness, central blindness, and swallowing difficulties, which correlated with 97% heteroplasmy.

1.6.4 *ATPAF2*

A homozygous T>A missense mutation was identified in *ATPAF2* (60), which is the nuclear gene that encodes the human Atp12p homolog. The mutation causes the replacement of an evolutionarily conserved tryptophan with arginine at position 94 of the mature protein with devastating consequences; the patient exhibited severe neonatal encephalopathy that led to basal

ganglia atrophy shortly after birth and death at 14-months. There was a significant decrease in the amount, and therefore the activity of ATP synthase in the patient. Plasmid-borne human *ATPAF2* had been shown to rescue the respiratory defect of $\Delta atp12$ yeast (61). Members of our laboratory took advantage of this fortunate circumstance and used the yeast model to characterize the effects of the W94R mutation in human Atp12p (62). The mutation was shown to alter the structure of Atp12p in a manner that compromised its solubility in mitochondria.

1.6.5 *TMEM70*

Transmembrane protein 70 is a mitochondrial protein that is encoded by the human *TMEM70* gene. Frameshift and splice site mutations in the *TMEM70* gene have been reported for patients among the homogenous ethnic group of Romani people (63). The common clinical manifestations of mutations in *TMEM70* include lactic acidosis, dysmorphic features, and encephalocardiomyopathy. There have also been additional complications such as early-onset cataract, gastrointestinal dysfunction, congenital hypertonia, and a fetal presentation of the syndrome associated to particular mutations (64). A milder version of the symptoms was observed in a patient with harboring splice site and missense mutations (65). Limited experiments have been interpreted to suggest that transmembrane protein 70 might regulate how much F_0 protein gets incorporated in the membrane, though the actual function of this protein in complex V biogenesis remains to be determined (66).

1.6.6 ATP synthase subunit epsilon: *ATP5E*

When an A>G homozygous missense mutation in exon 2 of human *ATP5E* ($F_1 \epsilon$ subunit) was reported in a patient, it was the first genetic lesion discovered in a nuclear gene that codes for a structural subunit of the ATP synthase. The resultant Y12C substitution in the ϵ subunit caused a decrease in mitochondrial complex V that was associated to neonatal onset of lactic

acidosis, 3-methylglutaconic aciduria, and mild mental retardation. In contrast to all of the other complex V mitochondrialopathies that have been described, the mutation in *ATP5E* was additionally correlated with the accumulation of the *c*-subunit in the membrane. Perhaps this is not surprising in view of work that has focused on the ϵ subunit of humans (67) and yeast (68), and the homologous δ subunit of bacteria (69), which revealed how important this protein is for the interactions between F_1 and the F_0 proton channel.

CHAPTER 2: MATERIALS AND METHODS

This section provides only the experimental details of work done by me with the *atp1* and *atp2* mutants. The PCR conditions and the oligonucleotide primers used by Dr. Xu to identify the nucleotide changes reported in the tables shown in Figure 5A are given in Appendix #.

Cells and Media

The *atp1* and *atp2* mutants were derived from the respiratory-competent haploid strain of *S. cerevisiae*, D273-10B/A1 (*MAT α met6*). Yeast were grown in the following media: YPD (2% glucose, 2% peptone, 1% yeast extract), YPGal (2% galactose, 2% peptone, 1% yeast extract), YEPG (3% glycerol, 2% ethanol, 2% peptone, 1% yeast extract), WO (2% glucose, 0.67% yeast nitrogen base without amino acids (Difco)). Amino acids and other growth requirements were added at a final concentration of 20 μ g/ml. *Escherichia coli* TB1 (*hsdR ara Δ (lac-pro AB) rpsL [Φ 80d lac (Δ lac Z)M15]*) was the host bacterial strain for recombinant plasmid constructions. Non-transformed bacteria were grown in LB (% glucose, % tryptone, % NaCl). Plasmid-bearing *E. coli* was grown in AMP medium (% antibiotic medium (Difco) plus Ampicillin at 40 μ g/ml final concentration. Solid media included 2% agar.

Preparation of yeast mitochondria

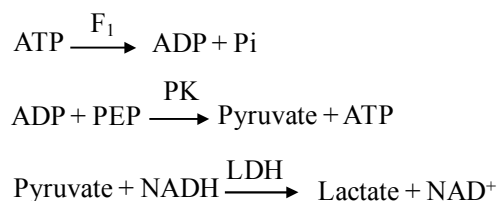
Yeast were grown aerobically in liquid YPEG or YPGal at 30° C to early stationary phase. The method of Faye *et al* (70) was used to prepare mitochondria with the exception that Zymolase, instead of Glusulase was added to digest the cell wall. Digestion was monitored using a light microscope to examine small aliquots, which had been diluted on the slides with water, for changes in morphology (e.g. clumping) and hypo-osmotic lysis (e.g. excessive cell debris). In brief, the isolation of mitochondria from spheroplasts proceeded with mechanical shearing of cells in 30 ml volumes of buffered 0.5 M sorbitol using a Waring blender equipped

with a stainless steel 50 ml mini-cup. Phenylmethylsulfonyl fluoride (PMSF) dissolved in EtOH was added to 10 $\mu\text{g/ml}$ final concentration just prior to homogenization to minimize proteolysis. The homogenate was centrifuged at $\sim 2500\times g$ to remove nuclei and unbroken cells and the clarified suspension was then centrifuged at $15,000\times g$ to pellet mitochondria. After washing twice, mitochondria were suspended routinely using a dilute Tris-HCl buffer (10 -20 mM) buffered at pH 7.5. Protein concentration was estimated using the *Lowry* procedure (71). The final yield of mitochondria from an 800ml culture was 10-13 mg (0.5-0.6 ml at 20 mg/ml). The yields from mutant cultures were variable, but typically did not dip below 3-4 mg.

ATPase assays

ATPase activity was measured, in the absence and presence of oligomycin, using a coupled enzyme assay (72) (Scheme 1).

Scheme 1



Assays were performed with a Cary 100 UV/VIS spectrophotometer and monitored the sample for absorbance change at 340 nm. A Fisher Scientific (Model Isotemp 3016) circulating water bath attached to the instrument maintained the temperature of the sample compartment constant at 30° C. The sample cuvette contained 1 ml of reaction mixture (2 mM Phosphoenol pyruvate, 4 mM ATP, 0.3 mM NADH, 320 μg Pyruvate kinase, and 130 μg Lactate dehydrogenase). Following the addition of 5 μl EtOH (minus oligomycin conditions) or 5 μl oligomycin (stock concentration) (plus oligomycin conditions), the assay was initiated by the addition of mitochondria (volume range 1-50 μl) and data collected for 2 minutes. Slopes ($\Delta\text{O.D./min}$) were

calculated from the linear region of the traces (CARY software version) and the decrease in NADH concentration was determined by dividing the slopes by the extinction coefficient (6.23 mM^{-1}). Since all of the reaction components are present at 1:1 stoichiometry, $\mu\text{mole NADH}$ consumed per minute is equal to $\mu\text{mole Pi}$ produced per minute (reaction velocity; expressed as U (standard unit of enzyme activity)). F_1 activity is reported as Specific Activity ($\mu\text{mole min}^{-1} \text{ mg}^{-1}$ or U mg^{-1}), which was calculated by dividing the velocities by the total amount of mitochondrial protein (mg) in the 1 ml assay.

Extraction of F_1F_0 from mitochondria

Mitochondria were suspended at 5 mg/ml in a buffer containing 10 mM Tris-HCl, pH 8.0, 4 mM ATP and 1 mM EDTA at volumes ranging from 150 - 200 μl . Triton X-100 was added to a final concentration of 0.25%, and PMSF (final concentration 10 $\mu\text{g/ml}$) was added to minimize proteolysis of the solubilized proteins. After removing an aliquot (30-40 μl) to a 4X SDS solubilization (Laemmli) solution, the rest of the mixture was incubated at 0°C on ice and then centrifuged at 100,000 g for 30 min at 4°C . The supernatant was removed to a fresh tube and the insoluble material was suspended in buffer back to the pre-centrifugation volume. Samples of the freshly isolated soluble and particulate fractions were mixed with 4X Laemmli solution and stored at -20°C . The remaining fractionated material was kept frozen at -70°C .

Step sucrose centrifugation analysis of F_1 -ATPase subunits

Mitochondria were suspended at 5 mg/ml in a buffer containing 10 mM Tris-HCl, pH 8.0, mM ATP and 1 mM EDTA at a volume of 200 μl . Triton X-100 was added to a final concentration of 0.25%, and PMSF (final concentration 10 $\mu\text{g/ml}$) was added to minimize proteolysis of the solubilized proteins. An aliquot of the sample (30 μl) was added to a 4X SDS-sample buffer solution (Laemmli). The remaining mixture was incubated at 0°C on ice for 20

min, and the entire volume was overlaid on top of a discontinuous gradient of 10 mM Tris HCl (pH 7.5)-buffered sucrose built from 1.2 ml of 80%, 0.9 ml of 60%, 0.9 ml of 50%, 0.9 ml of 30%, and 0.9 ml of 20% sucrose. The gradients were centrifuged at 36,000 g for 2 hr 30 min in a Beckman SW-55Ti rotor, and 10 fractions were collected from the bottom of the tube. Equivalent volumes (45 μ l) of each fraction were mixed with 4X Laemmli solution and stored at -20° C for western analysis. The remaining volumes of the sucrose gradients were stored at -80° C.

Linear sucrose centrifugation analysis of soluble F₁F₀

Linear sucrose gradients were used to evaluate the size of the F₁F₀ complex in mitochondrial supernatants. Mitochondria were suspended at 5 mg/ml in a buffer containing 10 mM Tris-HCl, pH 8.0, mM ATP and 1 mM EDTA at volume ranges of 600-800 μ l. Triton X-100 was added to a final concentration of 0.25%, and PMSF (final concentration 10 μ g/ml) was added to minimize proteolysis of the solubilized proteins. The entire mixture was incubated at 0° C on ice for 20 min and centrifuged at 100,000xg for 30 min at 4° C. An aliquot of the supernatant fraction (30 μ l) was mixed with 4X SDS-sample buffer (Laemmli), and the remaining volume (0.6 ml) was loaded onto a 4.4 ml 6-20% sucrose gradient prepared in 0.1% Triton X-100 supplemented TEA buffer. The gradients were centrifuged at room temperature for 1.5 h at 36,000 g in a Beckman SW55Ti rotor. For all the experiments, twenty fractions of equivalent volumes were collected from the bottom of the tube and 15 μ l of the sample was analyzed to detect the F₁ α and β subunits by western analysis as outlined in the “Western blotting analysis” section.

Western blotting analysis

Mitochondrial samples mixed with 4X SDS-sample buffer containing 60 mM Tris pH 6.8, 50% glycerol, 10% SDS, and 14.4 mM β -mercaptoethanol was heated at 95° C for 5 min. 30 μ g of protein samples were resolved electrophoretically using a 12% SDS- polyacrylamide reducing gel in a buffer containing 250mM Tris base, 1.9 M glycine, and 10% SDS. Following electrophoresis, the SDS gels, nitrocellulose membranes (0.45 μ m, Amersham Protran), and filters papers of equivalent sizes were immersed in a transfer buffer (25 mM Tris base, 191 mM glycine, and 200 ml methanol) for 15 min to equilibrate. A transfer sandwich was prepared and the proteins were transferred from the gel to nitrocellulose membrane in the same transfer buffer at a constant voltage of 100 V for 40 min. The transferred proteins were stained with Ponceau S to visualize the bands. The desired bands were marked for identification and destained by washing with Tris-buffered saline containing 20 mM Tris-HCl, 0.5 M NaCl, and 0.1% Tween 20 (TBS-T) for 5 min. The nitrocellulose membrane was incubated with 10 ml of 1.5% (w/v) non-fat dry milk in TBS-T for one hour to eliminate non-specific binding. The membranes were probed with a primary antibody for 1 h with shaking at 25° C, followed by 3 washes of TBS-T (10 min per wash) to remove any unbound primary antibody. It was then incubated with the corresponding secondary antibody conjugated to horseradish peroxidase (HRP) for 30 min with shaking at 25° C. After the secondary antibody treatment, the membrane was washed 3 times with TBS-T (10 min per wash) to eliminate any unbound antibody that may contribute to a background signal. The blot was incubated in a solution containing luminol (Clarity™ Western ECL) for 5 min. The oxidation of luminol by HRP produces 3-aminonaphthalate, which on decay emits light and produces a signal when exposed to an X-ray film.

For the analysis of the F₁ subunits from the linear sucrose gradient fractions, the proteins were precipitated using trichloroacetic acid (TCA) prior to western analysis. Briefly, 1 volume of TCA (66.6 μ l) was added to 4 volumes (~250 μ l) of the protein sample and incubated at 0° C on ice for 20 min. The protein samples were centrifuged at 13,000 rpm for 5 min in a benchtop centrifuge (Biofuge). The supernatant fraction was discarded and the pelleted fractions were washed with 200 μ l of ice-cold Acetone. The samples were centrifuged at 13,000 rpm for 5 min to discard the acetone. This wash step was repeated twice to rid the protein samples of any residual TCA. The pellets were dried by placing the tubes in a 95° C heat block for 2 min to drive off the acetone. The samples were mixed with 25 μ l of 1X SDS-sample buffer and resolved on a 12% SDS-polyacrylamide reducing gel electrophoretically. The remainder of the procedure for western analysis is as described above.

Yeast transformations

Yeast strains were inoculated on a fresh YPD plate and incubated for 1-2 days at 30 ° C. After a substantial amount of growth on the YPD plate, a loopful of the yeast strain was transferred aseptically in 10 ml of TE buffer containing 10 mM Tris-HCl pH 7.5, and 1mM EDTA. The yeast cells were centrifuged at 5000 g (Sorvall GLC) for 5 min to wash off any contaminants that may be present. The cells were re-suspended in 10 ml TEL (10 mM Tris pH 7.5, 1 mM EDTA, 0.1 M lithium acetate). The cells were centrifuged in a Sorvall SA-600 rotor at 17,000 g for 5 min and the supernatant was discarded. A carrier DNA (Salmon sperm DNA) is essential for the transformation of plasmids into yeast cells and the Lithium Acetate (LiAc) protocol requires it to be single stranded. To achieve this, salmon sperm DNA (10 mg/ml) was warmed at 90 ° C for 2 min to denature the DNA and then put at 0° C on ice to avoid the DNA from re-annealing. The cell pellets were suspended in 0.1 ml TEL and transferred to a sterile 1.5

ml microcentrifuge tube. Transforming DNA (1-10 μg) was added directly to 5 μl of the carrier DNA and mixed well with the yeast cells followed by incubation at 25° C for 30 min without shaking. After incubation, 40% of polyethylene glycol 4000 (700 μl) was added to the cells and mixed with a pipettor. The mixture was incubated at 25° C for 1 h and then heat shocked at 45° C for 10 min. Li^{2+} , PEG, and heat shock are absolutely necessary for the entry of the plasmid into yeast cells (73). The cells were centrifuged at 13,000 rpm for 1 min and the supernatant was discarded. They were re-suspended in 200 μl of sterile TE and centrifuged at 13,000 rpm for an additional 1 min (2 times). The yeast pellets were finally re-suspended in 400 μl of TE and 200 μl was spread on a selective medium and incubated at 30° C for 2 days.

In the case of Geneticin (G418) as a selection media, the protocol for yeast transformation is similar to the one described above, except for the last step which is modified as follows: The yeast cells that were washed with 200 μl of TE were re-suspended in 1 ml YPD media and incubated at 30° C with shaking for 16 h. 100 μl of the cultured cells were spread on a G418 plate (YPD with 0.2 mg/ml G418) and incubated at 30° C for 2 days.

Lactate dehydrogenase (LDH) assay

LDH was used as a molecular weight marker to determine the size of the $\alpha\beta$ dimers in the linear sucrose fractions of the *atp2* yeast mutant E323. Mitochondria were suspended at 5 mg/ml in a buffer containing 10 mM Tris-HCl, pH 8.0, mM ATP and 1 mM EDTA at volume ranges of 600-800 μl . Triton X-100 was added to a final concentration of 0.25%, and PMSF (final concentration 10 $\mu\text{g}/\text{ml}$) was added to minimize proteolysis of the solubilized proteins. The entire mixture was incubated at 0° C on ice for 20 min and centrifuged at 100,000 \times g for 30 min at 4° C. An aliquot of the supernatant fraction (30 μl) was mixed with 4X SDS-sample

buffer (Laemmli). To the remaining volume (0.6 ml), 1 μl (2.75 U/ μl) of LDH was added from a stock solution of 5 mg/ml (550 U/mg) and mixed well. The entire volume was loaded onto a 4.4 ml 6-20% sucrose gradient prepared in 0.1% Triton X-100 supplemented TEA buffer. The gradients were centrifuged at room temperature for 1.5 h at 36,000 g in a Beckman SW55Ti rotor. For all the experiments, twenty fractions of equivalent volumes (250 μl) were collected from the bottom of the tube. The reaction for the LDH assay is depicted below (Scheme 2).

Scheme 2



Assays were performed with a Cary 100 UV/VIS spectrophotometer and monitored for absorbance change at 340 nm. A Fisher Scientific (Model Isotemp 3016) circulating water bath attached to the instrument maintained the temperature of the sample compartment constant at 30° C. Before initiating the assay, the sample and the reference compartments were blanked using 20 mM Tris-HCl, pH 7.5. The sample cuvette containing 1 ml of reaction mixture (0.2 M Tris-HCl, 0.2 mM NADH, 1 mM Pyruvate) shows an O.D. of 1.25 which corresponds to the concentration of NADH in the reaction mixture. The assay was initiated by the addition of the eluted soluble fractions (volume range 1-10 μl) and data collected for 2 minutes. Slopes ($\Delta\text{O.D./min}$) were calculated from the linear region of the traces (CARY software version) for each of the 20 fractions. To determine the peak of the LDH in the linear sucrose gradient, a graph of slope ($\Delta\text{O.D./min}$) v/s fraction number was plotted. The fraction number that shows the highest slope for the reaction indicates the position of the LDH in the gradient.

CHAPTER 3: CHARACTERIZATION OF MUTATIONS IN NUCLEAR GENES ENCODING THE α -SUBUNIT OR β -SUBUNIT OF YEAST MITOCHONDRIAL F₁

Summary

ATP1 and *ATP2* are yeast nuclear genes that code for the α subunit and the β subunit, respectively, of the mitochondrial F₁ component, which is the catalytic domain of the ATP synthase. Despite sharing only ~20% sequence identity, the three-dimensional fold of these proteins is essentially the same. Both proteins are synthesized in the cytoplasm as longer precursors with a targeting signal at the amino terminus that is removed once they have been imported to the mitochondrial matrix. In the assembled ATP synthase, the α and β subunits occupy alternating positions in the globular sub-domain of the F₁ $\alpha_3\beta_3\gamma\delta\epsilon$ oligomer (see Fig. 3 above). Chaperone-mediated assembly of the hexamer brings together amino acid side chains from each of the two proteins to create shared adenine nucleotide binding sites in cavities located at the six interfaces. Every other adenine nucleotide binding site is located primarily inside the β subunits, and these coincide with the active sites for F₁ catalysis. The other 3 sites reside largely in the α subunits, and are non-catalytic. Both the α and β subunits contain short spans of sequence called P-loops, also known as Walker motifs (74), which are essential to the adenine nucleotide binding capacity of the proteins. Among the conserved amino acids in these cavities, 3 P-loop amino acids in the β subunit are critical for the catalytic properties of this protein (19, 75, 76). In yeast, these correspond to G161, K162, and T163, and the only known functional variation has serine in place of the threonine residue (77). Another invariant amino acid is E188, which serves as the catalytic base for the ATP hydrolysis reaction (19). Notably, Q208 occupies the position in the α subunit that aligns with β -E188. Without the carboxylate group, Q208

cannot accept a proton, which explains why the adenine nucleotide binding sites in the α subunit are not catalytically competent (19).

F₁ α subunit mutants

Strain	Nucleotide change ^a	Codon change	Amino acid change ^b
P13	38 731	AGA→AAA GGA→GAA	R13K G244E
P26	557	GGT→GAT	G186D
P78	557	GGT→GAT	G186D
E594	604	GAG→AAG	E202K
E793	619	GAT→TAT	D207Y
E552	632	GGT→GAT	G211D
E559	632	GGT→GAT	G211D
C231	872	GGT→GAT	G291D
C273	1066	GGT→CGT	G356R
C258	1148	ACC→ATC	T383I
P263	1148	ACC→ATC	T383I
C67	1198	CCT→TCT	P400S
P164	1373	GGT→GAT	G458D
N112	1399	CAA→TAA	Q467Stop
N177	1432	CAG→TAG	Q478Stop

^aNucleotide sequence is numbered according to the wild type *ATP1* gene of *S. cerevisiae* strain S288c (NCBI accession number NM_001178339.2).

^bAmino acids are numbered beginning with the initiator methionine residue.

F₁ β subunit mutants

Strain	Nucleotide change ^a	Codon change	Amino acid change ^b
N294	106 509	GCT→ACT GGT→GAT	A36T G170D
E618	170	CAT→CCT	H57P
C166	244 1393	GAA→AAA GTG→ATG	E82L V465M
E636	536 1223	CCT→CTT CAA→CGA	P179L Q408R
E892	578	GGT→GAT	G193D
E397	668	AGA→AAA	R223L
N15	680 1405	GGT→GAT GAC→AAC	G227D D469N
E58	680	GGT→GAT	G227D
E677	680	GGT→GAT	G227D
P309	917 1024	GGT→GAT GCC→ACC	G306D A342T
E323	968	GGT→GAT	G323D
E312	1136	CCT→CTT	P379L
E873	1234	CAG→TAG	Q412Stop
N189	1332	CAA→CAC	Q444Y
N115	1343	TCT→TTT	S448F
E133	1446	TAC→TAA	Y482Stop

^aNucleotide sequence is numbered according to the wild type *ATP2* gene of *S. cerevisiae* strain S288c (NCBI accession number NM_001181779.3).

^bAmino acids are numbered beginning with the initiator methionine residue.

^cPoor cell growth precluded studies with isolated mitochondria.

Figure 5A. Mutant genes cloned and sequenced from *atp1* and *atp2* yeast strains belonging to complementation groups (G50, G1) of respiratory-deficient nuclear mutants.

The Tzagoloff collection of respiratory deficient yeast nuclear mutants includes complementation groups that were assigned to *ATP1* and *ATP2* (3). A former graduate student in the laboratory, Yueling Liang, cloned the mutant genes from 6 of the available 22 *atp2* mutants by colony hybridization, sequenced the mutations herself, and characterized the

properties of the corresponding mutant strains (78). Since then, the only significant work with the *atp1* and *atp2* strains was done by a former postdoctoral researcher in the lab, Dr. Xingie Xu. Dr. Xu used the polymerase chain reaction (PCR) to isolate the mutant genes from the *atp1* strains, as well as the remaining *atp2* mutants, and provided the DNA fragments to external vendors for sequencing. The mutations are described in the tables shown in Figure 5A.

It was at this stage that I began work on this project. My goal has been to determine the biochemical characteristics of the ATP synthase in the mutants and to determine if the overproduction of Atp12p in *atp1* yeast, or of Atp11p in *atp2* mutants, restored respiratory competence to any of them.

Results

Determination of oligomycin-sensitive ATPase activity in the *atp1* and *atp2* mutants

ATP synthases are able to catalyze phosphoryl transfer between ADP and water in both directions. Under normal physiological, the reaction runs only in the direction of ATP synthesis

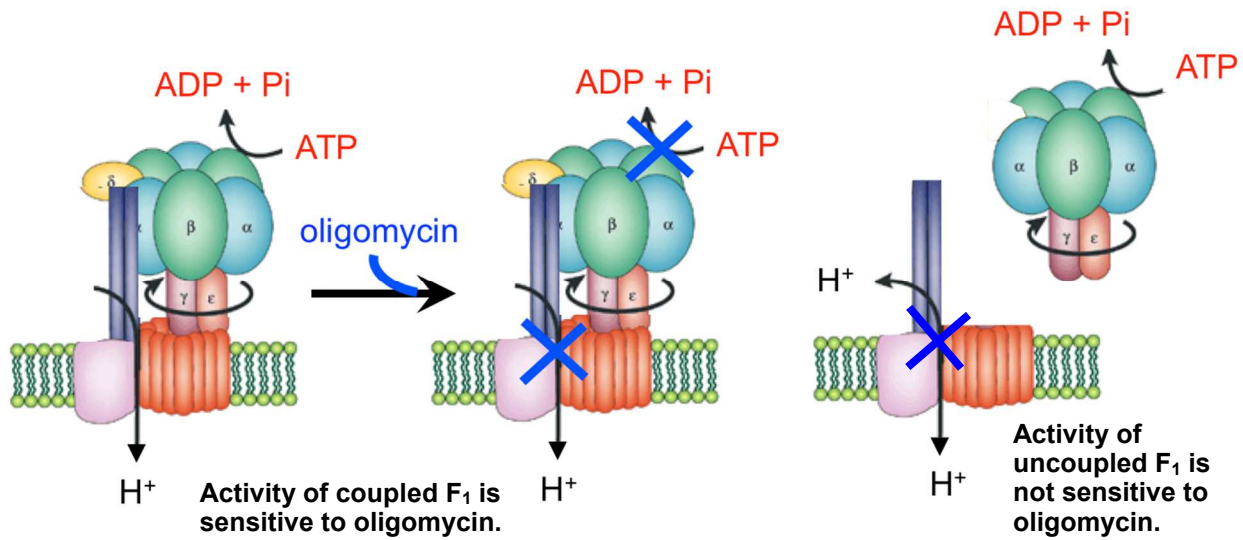


Figure 5B. Oligomycin distinguishes F_1 that is coupled F_0 from uncoupled F_1 . The cartoon image of the F_1F_0 from (99) was duplicated and modified to make this figure.

due to the presence of an inhibitory protein, IF1 in humans and Inh1p in yeast (Table 1), which prevents the enzyme from hydrolyzing ATP and wasting energy. The F_1 inhibitors associate stably with the enzyme under the mildly basic conditions that exist at the matrix face of the mitochondrial inner membrane. However, the association is lost during mitochondrial isolation from cells. Since it is much easier to measure ATP hydrolysis than ATP synthesis *in vitro*, investigators routinely employ an ATPase assay to evaluate the activity of the mitochondrial ATP synthase. Just as protons flow through F_0 during ATP synthesis in the F_1 domain, they do as well when ATP is hydrolyzed, albeit in the opposite direction (Figure 5B). In fact, the partial activities of proton transfer across the membrane and ATP hydrolysis are obligatorily linked; one cannot occur without the other. This relationship is commonly referred to as “coupling”, and

ATP hydrolysis by membrane-bound F_1 is described as being coupled to proton translocation. Oligomycin, a natural macrolide isolated from *Streptomyces diastatochromogenes*, is a highly specific inhibitor of mitochondrial ATP synthases. Oligomycin binds directly to the c -ring (79) in the membrane and prevents the translocation of protons through F_0 . ATP hydrolysis by the F_1 domain is likewise inhibited because of the coupling phenomenon (Fig. 5B, middle). Instead, if not bound to the membrane sector, the ATPase activity of free, soluble F_1 is completely resistant to oligomycin. Since oligomycin sensitivity is observed only if the F_1 domain is physically connected to the F_0 sector, oligomycin-sensitive ATPase activity is indicative that the ATP synthase is properly assembled. The ATPase activity was measured in preparations of

Table 2. ATPase activities of *atp1* mutants^a.

Strain	ATPase activity	
	Minus Oligomycin	Plus Oligomycin
	<i>μmole of NADH consumed/min/mg</i>	
D273	1.62 ± 0.23	0.47 ± 0.15
E552	0.22 ± 0.01	0.14 ± 0.01
E594	0.21 ± 0.02	0.15 ± 0.01
E559	0.30 ± 0.03	0.12 ± 0.01
P78	0.11 ± 0.07	0.05 ± 0.04
P13	0.12 ± 0.01	0.07 ± 0.02
P26	0.09 ± 0.01	0.04 ± 0.01
E793	0.26 ± 0.01	0.15 ± 0.03
C273	0.17 ± 0.01	0.08 ± 0.01
N112	0.10 ± 0.03	0.06 ± 0.01
C231	0.10 ± 0.01	0.07 ± 0.02
C67	0.10 ± 0.04	0.05 ± 0.01
P263	0.31 ± 0.01	0.14 ± 0.03
P164	0.21 ± 0.04	0.04 ± 0.01
C258	0.27 ± 0.02	0.09 ± 0.01

^aThe mean values are reported ± the standard error of the mean. See text for details.

mitochondria from the *atp1* mutants (Table 2) and from the *atp2* mutants (Table 3) as described under “Materials and Methods”. Each assay was done in duplicate, in the absence and presence of oligomycin, and the minus” and “plus” oligomycin values were averaged. The assays were performed with three independent mitochondrial preparations for each mutant, and the averaged values from each preparation were used to calculate the mean values (\pm the standard error of the mean) reported in Tables 2 and 3. The amount of oligomycin added to the assay was sufficient to inhibit ~70% of ATP hydrolysis in samples from the wild type yeast.

Table 3. ATPase activities of *atp2* mutants^a.

Strain	ATPase activity	
	Minus Oligomycin	Plus Oligomycin
	<i>μmole of NADH consumed/min/mg</i>	
D273 (WT)	1.62 \pm 0.23	0.47 \pm 0.15
E133	0.08 \pm 0.01	0.05 \pm 0.02
E636	0.10 \pm 0.04	0.07 \pm 0.02
E802	0.04 \pm 0.01	0.04 \pm 0.01
N115	0.09 \pm 0.01	0.06 \pm 0.02
E312	0.07 \pm 0.02	0.04 \pm 0.01
E397	0.14 \pm 0.04	0.08 \pm 0.01
C166	0.09 \pm 0.02	0.05 \pm 0.02
N294	0.34 \pm 0.09	0.19 \pm 0.01
N189	0.13 \pm 0.02	0.08 \pm 0.01
E892	0.11 \pm 0.03	0.08 \pm 0.02
E618	0.11 \pm 0.01	0.07 \pm 0.01
E677	0.14 \pm 0.01	0.09 \pm 0.02
E58	0.23 \pm 0.03	0.11 \pm 0.02
E323	0.04 \pm 0.02	0.03 \pm 0.01
N15	0.75 \pm 0.12	0.31 \pm 0.01

^aThe mean values are reported \pm the standard error of the mean. See text for details.

With one exception, the amount of ATPase activity, in the absence of inhibitor, was at or barely above the background level and this was interpreted to indicate these yeast have no functional mitochondrial F₁, coupled or uncoupled. N15, which is an *atp2* mutant, was the

outlier and showed nearly 40% the level of oligomycin-sensitive ATPase relative to wild type. N15 was among the mutant strains that were shown to harbor two mutations in the *ATP2* gene (G227D and D469N, see tables in Fig. 5A). The former (G227D) was identified as the sole mutation in the *ATP2* gene from two independent isolates in the same complementation group (E58 and E677) where it was correlated with a profound defect in ATP synthase assembly (described below). A model that shows how the D469N substitution might suppress the deleterious effect of the G227D mutation is presented under the Discussion.

Effects of mutations in *ATP1* or in *ATP2* on F₁F₀ solubility from the membrane

The ATPase assays revealed that nearly all of the *atp1* and *atp2* mutants were completely deficient for a catalytically-active ATP synthase, but provided no information about the status of ATP synthase assembly in the mutants. An easily tested characteristic of assembled F₁F₀ is that 30-40% of the enzyme can be solubilized from the mitochondrial membrane with 0.25% Triton X-100. A brief description of how this assay was adapted to characterize the ATP synthase in the *atp1* and *atp2* mutants is presented here; additional details are provided under the appropriate subheadings of Materials and Methods. Samples of mitochondria from the wild type (D273) and mutant yeast strains were adjusted to 5 mg/ml with 10 mM Tris-HCl, pH 8.0, 4 mM ATP, 1 mM EDTA, 0.25% Triton X-100 in a final volume of 200 μ l, incubated on ice for 20 min, and centrifuged in thick-walled 3 ml tubes in a Beckman 70.1 Ti rotor at 4° C (100,000 *g*, 30 min). Equivalent volumes of SDS-denatured total mitochondria (*M*), supernatant (*S*) and resuspended pelleted (*P*) fractions were run on 12% polyacrylamide gels (SDS-PAGE). The resolved proteins were transferred to nitrocellulose and the blots were incubated with polyclonal F₁ antibodies (isolated from chicken egg), washed, and treated with HRP conjugated secondary antibody (goat/anti-chicken). Finally, the blots were incubated with a chemiluminescent substrate for HRP

and used to expose X-ray film to locate the position of immunoreactive proteins. The experiments were performed with samples from at least two independent mitochondrial preparations for each yeast strain. Representative examples of the F₁ solubility profile are shown for the *atp1* mutants (Figure 6) and for the *atp2* mutants (Figure 7).

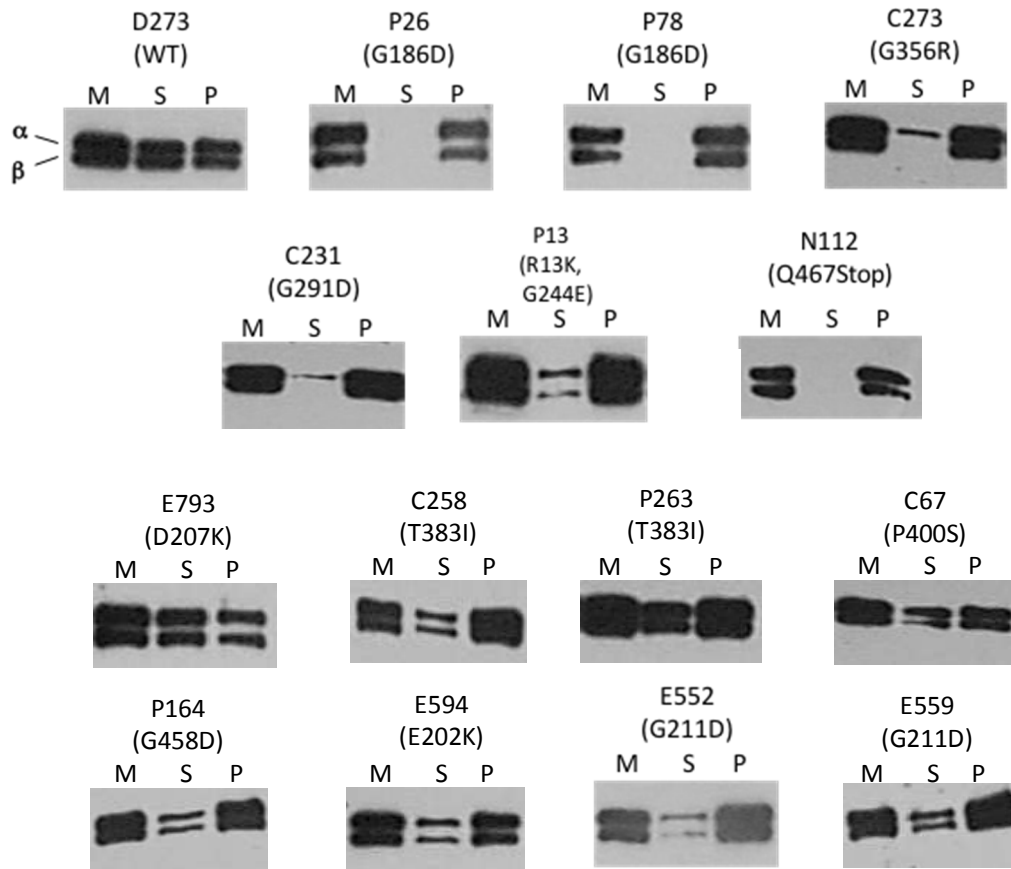


Figure 6. Western blots of F₁ α and β subunits in Triton X-100 extracted mitochondria from *atp1* mutants.

Aliquots of total mitochondrial protein (M), and equivalent volumes of the particulate (P) and soluble (S) fractions collected after treatment with 0.25% Triton X-100, were analyzed in Western. Blots using polyclonal antibodies against the yeast α and β subunits. The migration of the F₁ proteins is indicated top left for the data from the D273 wild type.

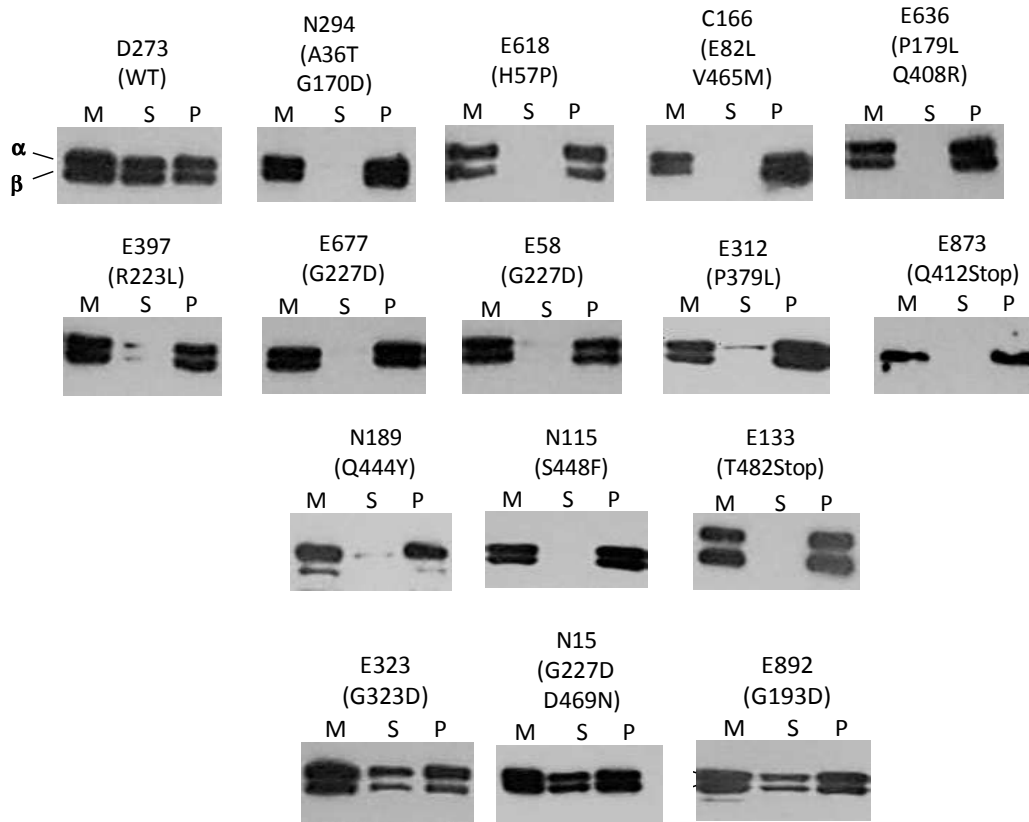


Figure 7. Western blots of F₁ α and β subunits in Triton X-100 extracted mitochondria from *atp2* mutants.

Aliquots of total mitochondrial protein (M), and equivalent volumes of the particulate (P) and soluble (S) fractions collected after treatment with 0.25% Triton X-100, were analyzed in Western. Blots using polyclonal antibodies against the yeast α and β subunits. The migration of the F₁ proteins is indicated top left for the data from the D273 wild type.

Compared with the results for the wild type, which showed near equal distribution of the F₁ α and β subunits between the supernatant and the pellet, there was essentially no F₁F₀ partitioned to the soluble fraction in the samples from yeast that harbor a subset of the *atp1* missense mutations (G186D (strains P26 and P78); E202K (strain E594); G291D (strain C231); G356R (strain C273)) or a nonsense mutation (Q467* (N112) and Q478* (N177, data not shown)). The results with the sample from P13 (R13K+G244E mutations) was less obvious, but the fact that the α : β subunit ratios in the solubilized protein fraction was consistently found to be not stoichiometric suggests that also in this mutant the F₁ component is not assembled properly. The results for mitochondrial samples from the *atp2* yeast were even more dramatic in this

respect, with all but 3 of the 14 newly identified mutant alleles correlating with the absence of F_1 protein in Western blots of Triton X-100 extracts (Fig. 7, rows 1-3, excluding wild type).

Overall, the F_1F_0 solubility profile for the 7 *atp1* mutants shown in the upper half of Fig. 6, and for the 12 *atp2* mutants in the top 3 rows of Fig. 7, is similar to what has been observed for $\Delta atp1$, $\Delta atp2$, $\Delta atp11$, and $\Delta atp12$ yeast, the latter of which were shown previously to accumulate the F_1 α and/or β subunits as aggregated proteins inside mitochondria (27); (described under section 1.4 of the Introduction). Density gradient centrifugation confirmed the presence of such aggregates in these subsets of *atp1* and *atp2* mutants. For these experiments, samples of Triton X-100 treated whole mitochondria (200 μ l) were loaded on top of 4.8 ml step gradients comprised of buffered sucrose solutions that were dispensed, from bottom to top, in layers of increasing concentration: 80%, 60%, 50%, 30%, 20%. The gradients were prepared in ultra-thin 5 ml tubes designed for the Beckman SW55 Ti swinging bucket rotor. These centrifuge tubes offered the advantage of permitting fractions to be collected by gravity through a small hole made in the bottom, after centrifugation was performed at 36,000Xg for 2.5 h. Samples for SDS-PAGE were prepared from the 10 fractions (500 μ l) collected for each gradient and analyzed in duplicate Western blots. One blot was probed with the antibody against F_1 and the other with polyclonal anti-cytochrome *c1* rabbit serum. Cytochrome *c1* is an integral membrane protein subunit of respiratory complex III that remains embedded in the membrane when mitochondria are exposed to 0.25% Triton X-100. As such, the position of cytochrome *c1* in the step sucrose gradient marks the position of inner membrane vesicles, which have the opportunity to reach the point of equal density ($\rho < 1.20$) at the applied g-force. When present, F_1 protein aggregates are so large in comparison to normal Triton X-100-extracted F_1F_0 (550 kDa)

that they reach the point of equilibrium for pure protein ($\rho > 1.26$; 60-80% sucrose boundary) within the time frame of the experiment (27).

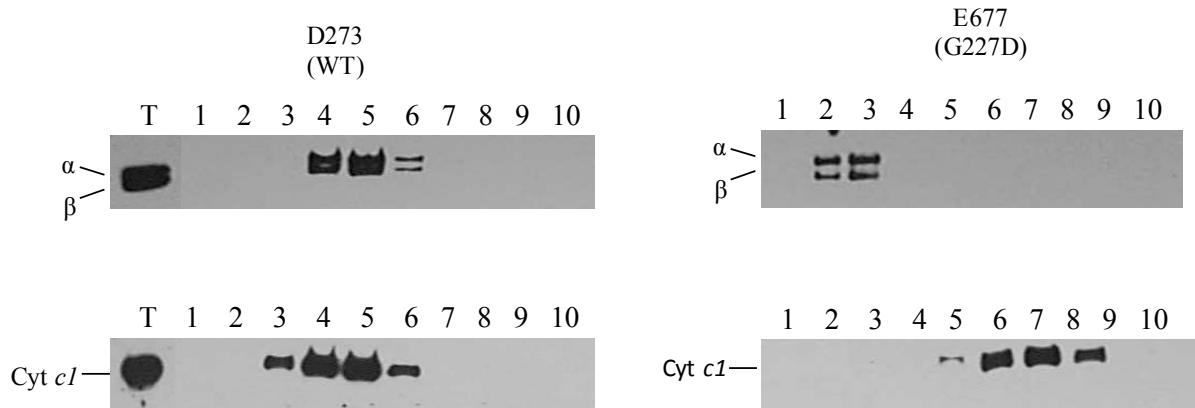


Figure 8. Western blots of step sucrose gradient fractions. Triton X-100 treated whole mitochondria from the wild type D273 (*left*) and the *atp2* mutant E677 (*right*) were centrifuged through a step sucrose gradient, and the 10 fractions obtained were analyzed on Western blots with antibodies against yeast F_1 or cytochrome *c1*.

The sedimentation profile for α and β subunits of F_1 in step sucrose gradients was practically identical for the mitochondrial samples from the *atp1* mutant strains P26, P78, E594, C231, C273, P13, and N112, and the *atp2* strains N294, E618, C166, E636, E397, E677, E58, E312, E873, N189, N115, and E133. The results for one of the mutant (E677) is presented here, along with the wild type control, to illustrate the concepts (Figure 8). The F_1 α and β subunits were observed to co-migrate with *cytc1* when Triton X-100 treated whole mitochondria from the wild type was centrifuged through a step sucrose gradient (Figure 8, *left blots*). There is only 1 peak for these proteins despite the fact the sample contains both solubilized and membrane-bound F_1F_0 . The F_1 protein sedimentation pattern was quite different for the detergent-treated mitochondria from the *atp2* mutant E677 (*right blots*). In this case the entire signal for F_1 protein was detected at the 60-80% sucrose boundary. This result shows that there is no F_1F_0 at all assembled in E677 mitochondria, and that all of the F_1 α and β subunit protein is aggregated.

One final point about these experiments deserves mention. The temperature of the rotor was maintained at 25° C during the centrifugation of the samples. This condition was chosen because, on its own, the isolated mitochondrial F₁ oligomer is cold-sensitive and denatures rapidly at 4° C (72). Hence, the sucrose gradient centrifugation methods that have been developed to investigate ATP synthase assembly are commonly carried out at room temperature (27, 80).

Novel assembly-defective phenotypes in *atp1* and *atp2* mutants

Two *atp2* mutants (E323 and E892) and approximately half of the *atp1* strains were found to be completely deficient for mitochondrial ATPase activity, but nonetheless showed evidence of F₁ protein that was released to the soluble fraction following the exposure of mitochondria to 0.25% Triton X-100. For these cases, the size of the solubilized protein was determined in experiments that evaluated its sedimentation through a linear gradient of sucrose (6-20%). Samples (600 µl) of the supernatants, obtained after Triton X-100 treated mitochondria were centrifuged at 100,000Xg for 30 min, were carefully overlaid 4.4 ml gradients and centrifuged in a Beckman SW55Ti rotor at the specified g-force. Twenty fractions (250 µl) were collected from the bottom of the centrifuge tubes, and the protein in each fraction was

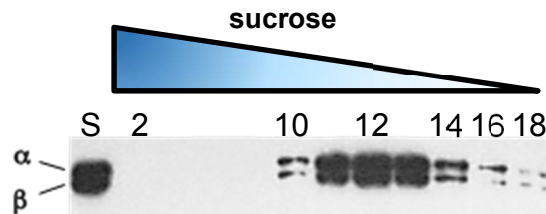


Figure 9. Sedimentation analysis of the F₁ protein in Triton X-100 extracts of mitochondria from the wild type D273.

Western blots of fractions from 6-20% linear sucrose gradients. An aliquot of the solubilized protein sample (S), pre-centrifugation, was loaded in the left-most lane to mark the position of the F₁ α and β subunits.

precipitated with 5% TCA to concentrate the samples. The precipitates were washed with acetone before being suspended in 25 μ l 1X SDS gel sample buffer. One microliter of unneutralized Tris was added to gel samples that were yellow to counter the residual acid. Equal volumes of the gel samples were evaluated in Western blots for the position of the F₁ α and β subunits. When the Triton X-100 solubilized proteins from wild type mitochondria were centrifuged at 36,000Xg for 1.5 h, the F₁F₀ complex peaked near the middle of the gradient in fraction 12 (Figure 9).

Instead, when the experiment was performed under identical conditions with the sample from E323, the F₁ protein peak was detected in a region of much lower sucrose density in fractions 16-20 (Figure 10A). The monomeric molecular weight of F₁ α and β is ~55 kDa and ~52 kDa, respectively, whereas an $\alpha\beta$ dimer is ~110 kDa. To better estimate the size of the soluble F₁ protein in mitochondria from E323, the experiment was repeated exactly the same way except that 2.75 units/ μ l of porcine heart lactate dehydrogenase (140,000 kDa) was mixed with the soluble protein sample before it was loaded on the gradient and the fractions were

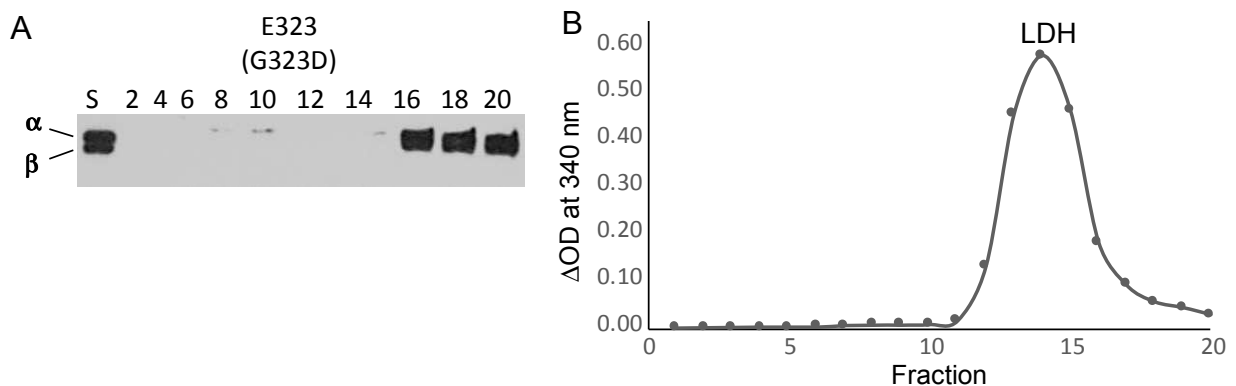


Figure 10. Sedimentation analysis of the F₁ protein in Triton X-100 extracts of mitochondria from *atp2* mutant E323.

A, Linear sucrose sedimentation profile of soluble fractions from *atp2* mutant E323. An aliquot of the solubilized protein sample (*S*), pre-centrifugation, was loaded in the left-most lane to mark the position of the F₁ α and β subunits. *B*, LDH assay to determine the relative size of the $\alpha\beta$ dimers that are observed in the linear sucrose gradients

probed for LDH activity as described under “Materials and Methods”. In the presence of pyruvate and NADH, LDH catalyzes pyruvate reduction to lactate concomitant with NADH reduction to NAD⁺. LDH activity in each fraction was determined spectrophotometrically by following the decrease in NADH absorbance at 340 nm for 2 min and the slopes (Δ O.D./time) were plotted versus fraction number (Fig. 10B). The LDH peak was detected in fraction 14, just ahead of the F₁ protein. This finding is consistent with an estimated size in the 100-120 kDa range for the F₁ protein in E323 mitochondria, and supports the idea that the *atp2* mutation G323D in E323 yeast causes F₁ assembly to stall at the point where $\alpha\beta$ dimers are formed. This was the first time an assembly defect of this type has been observed in our laboratory and it has not been reported in the literature.

When a linear sucrose gradient was performed with the sample from E892 (Figure 11A), the pattern of F₁ protein distribution was very different from both wild type (Fig. 9) and the E323 mutant (Fig. 10). There appeared to be one peak in fractions 8 and 9, and perhaps another accumulation in fraction 3. Moreover, the experiment had not captured protein complexes that were significantly larger than a single F₁F₀ molecule. The sieving action of linear gradients is similar to a gel filtration column in which proteins separate according to mass, with larger proteins eluting first. The intensity of the Western blot signals in the fractions from the bottom of the tube (lowest numbers) indicated that at the applied *g*-force, protein had passed all the way through the 20% sucrose solution and was out of the detectable range. Therefore, to ensure the full complement of F₁ protein would be visualized in the fractions collected, the preparation of the gradient was modified and a 3.9 ml linear 6-20% gradient was built on top of 0.5 ml 80% sucrose deposited at the bottom the tube. Since the density of 80% sucrose is greater than the density of pure protein (see above), F₁ protein complexes large enough to have passed through

20% sucrose under the previous centrifugation conditions were captured in fraction 3 at the 20/80% sucrose interface (Fig. 11B). Moreover, all of the Western blot signal was concentrated in a single peak in fractions 3-5.

Among the *atp1* mutants that showed evidence of detergent extractable F_1F_0 , further experiments showed that the biochemical phenotype of E793 (Figure 12) was very similar to E892, an *atp2* mutant. Under the same conditions of applied *g*-force, the E793 F_1F_0 peak migrated much further in a 6-20% sucrose gradient (Fig. 12A), compared to wild type F_1F_0 (Fig.

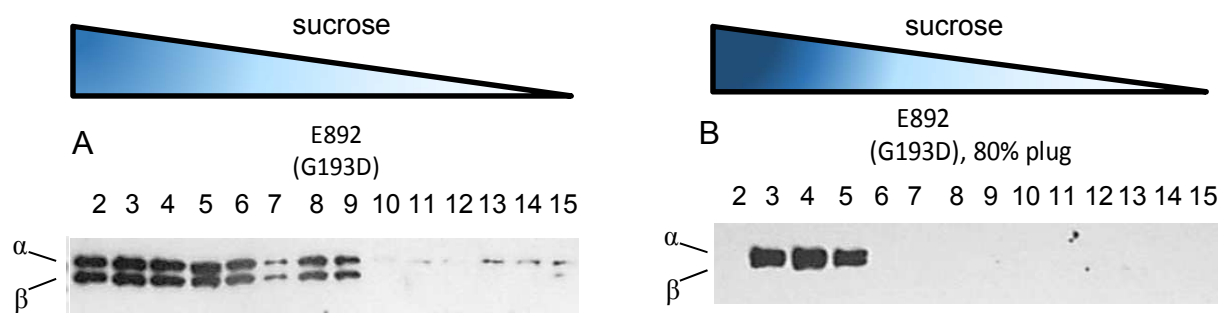


Figure 11. Sedimentation analysis of the F_1 protein in Triton X-100 extracts of mitochondria from *atp2* mutant E892.

A, Western blot of fractions collected after the solubilized protein from mutant E892 was centrifuged through a 6-20% sucrose gradient. *B*, Same as *A* except that the 6-20% linear gradient was built on top of 0.5 ml 80% deposited at the bottom of the centrifuge tube.

9), and could be condensed at the 20/80% sucrose interface (Fig. 12B). It is important to recall here that the E892 and E793 samples, which were analyzed on 6-20% linear gradients, had been first recovered in the *soluble fraction* after detergent-treated mitochondria was centrifuged to pellet membranes and large, particulate material such as the large insoluble aggregates of α and β subunits that were described above. The sedimentation patterns for solubilized F_1F_0 from E892 and E793 were different from anything that has been observed in our lab or reported by others. The effect of the D207Y mutation in the F_1 - α subunit or of the G193D mutation in the F_1 - β subunit appears to alter the structure of the F_1F_0 in a manner that leads to its

oligomerization in detergent extracts to structures that are larger than dimers. Particularly interesting is that each mutation maps to the P-loop subdomain in the adenine nucleotide binding cavity of the respective protein, which in the α subunit is between residues 206-213 (GDRQTGKT) and in the β subunit between residues 190-197 (GGAGVGKT). The

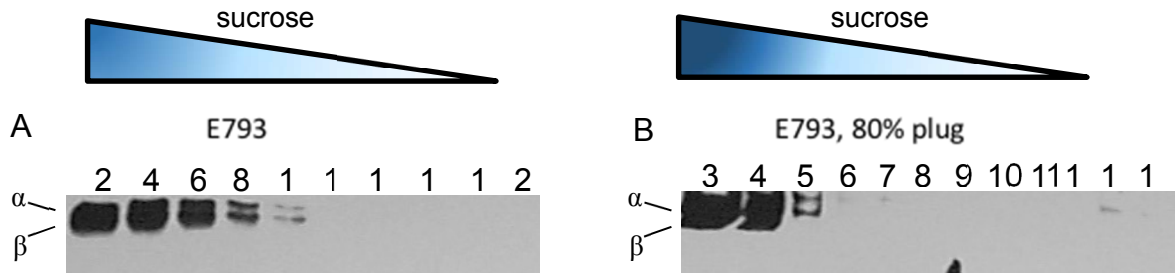


Figure 12. Sedimentation analysis of the F_1 protein in Triton X-100 extracts of mitochondria from *atp1* mutant E793.

A, Western blot of fractions collected after the solubilized protein from mutant E793 was centrifuged through a 6-20% sucrose gradient. *B*, Same as *A* except that the 6-20% linear gradient was built on top of 0.5 ml 80% deposited at the bottom of the centrifuge tube.

ramifications of these findings with respect to the fact that the cavity locations correspond to the $\alpha\beta$ interfaces in the F_1 hexamer are presented below under the Discussion.

The sedimentation patterns for the F_1F_0 that partitioned to the soluble fraction following

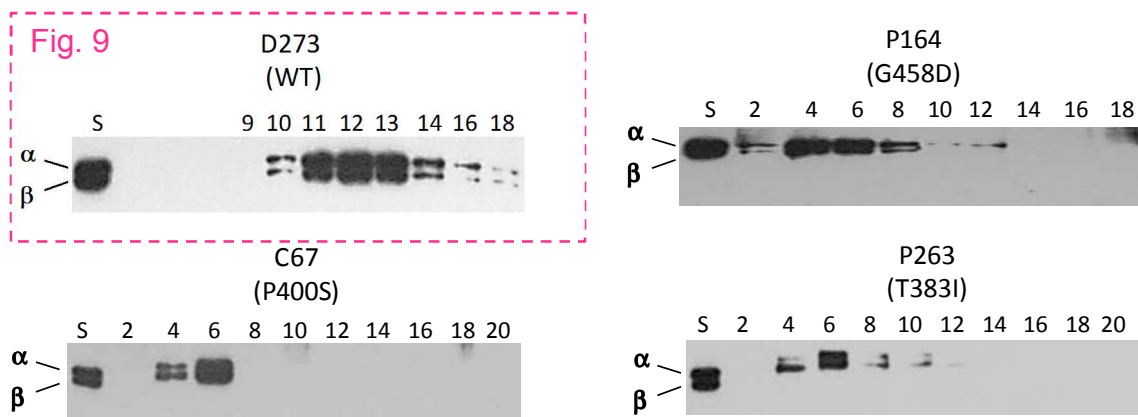


Figure 13. Sedimentation analysis of the F_1 protein in Triton X-100 extracts of mitochondria from additional *atp1* mutants.

Western blots of fractions collected after the solubilized protein from the *atp1* mutants P164, C67, and P263 were centrifuged through a 6-20% sucrose gradient. The image showing the result for D273 (pink box) was reproduced here from Fig. 9 for comparison. An aliquot of the solubilized protein sample (S), pre-centrifugation, was loaded in the left-most lane to mark the position of the F_1 α and β subunits.

centrifugation of Triton X-100 extracted mitochondria from the remaining *atp1* mutants (C258, P263, C67, P164, E594, E552, and E559) were similar to each other but different from wild type (Figure 13); to avoid redundancy, data is reported for 3 of the 7 mutants. The wild type profile reported in Fig. 9 was repeated in this figure (*pink box*) to facilitate its comparison with the mutants. The F_1F_0 complexes in these latter 7 strains were larger than wild type yet significantly smaller than the multimers observed for E793 and E892 (Figs. 11 and 12 above).

The G227D mutation in the *atp2* mutant N15 is suppressed partially by the additional D469N substitution in the protein

There was ~40% the normal amount of ATPase activity (Table 3) measured with mitochondria from the *atp2* mutant, N15, and extraction of the mitochondria with 0.25% Triton X-100 revealed wild type-like characteristics for F_1F_0 solubilization (Fig. 7). Furthermore, the

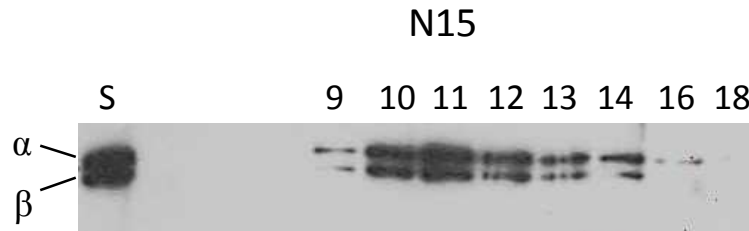


Figure 14. Sedimentation analysis of the F_1 protein in Triton X-100 extracts of mitochondria from *atp2* mutant N15. The N15 sedimentation profile is similar to the wild type protein and the F_1 subunits peak in the middle of the sucrose gradient.

sedimentation of detergent solubilized N15 F_1F_0 was shown to be comparable to the wild type protein (Figure 14). Nonetheless, N15 does not respire as indicated by the inability of this yeast to grow on non-fermentable carbons (EG plates). Previous work reported in the literature has shown that yeast displaying as little as 15% wild type levels of mitochondrial ATPase activity can grow on EG plates (81). Presumably such yeast also synthesize ATP at 15% the wild type rate and this is sufficient to confer growth on the selective medium. N15 harbors the same

mutation (G227D) as two other *atp2* mutants (E58, E677, see tables in Fig. 5A), the latter of which accumulate the F₁ α and β subunits in insoluble aggregates (Fig. 7). The difference is the presence of a second mutation (D469N) in the *ATP2* gene of N15. Cumulatively the results suggest that the D469N second-site mutation confers to N15 the assembly of an F₁F₀ complex that is structurally comparable to wild type, and partially catalytically competent. However, the EG minus phenotype indicates that ATP synthesis in this strain is below the threshold needed to support non-fermentative growth, and is not equivalent in magnitude to the level of ATP hydrolysis observed for the mutant enzyme.

Overexpression of *ATP11* and *ATP12* genes

Yeast plasmids were constructed that over-express the *ATP11* and *ATP12* genes in the *atp2* and *atp1* mutants respectively. The wild type *ATP11* (pG13/ST4) and *ATP12* (pG57/ST4) DNAs cloned in a high copy-number yeast expression plasmid were available in the laboratory. However, these plasmids have a *URA3* marker gene, which is not suitable for selection of the plasmids in strains derived from D273-10B/A1 (*MAT α met6*). Therefore, the plasmids pG13/ST4 and pG57/ST4 were modified to include the genetic module (KanMX) that confers resistance of yeast to G418, a drug that is similar to the antibacterial agent kanamycin. Both plasmids were digested with an enzyme that creates blunt ends (pG13/ST4 with *EcoRV*, and pG57/ST4 with *StuI*). The KanMX module was excised as a 1586 bp blunt ended DNA fragment from *PvuII*, *EcoRV* digested pUG6 (gift from Amy Roth, Department of Pharmacology), ligated with the linearized *ATP11* and *ATP12* plasmids, and used to transform *E.coli* TB1. Bacterial clones were selected on kanamycin and the plasmid maps were verified using restriction enzymes. The methods used to transform yeast with these plasmids and select on G418 media is described under “Materials and Methods”.

To ensure the new plasmids produced functional Atp11p or Atp12p proteins, pG13/ST4/KanMX and pG57/ST4/KanMX were used to transform the $\Delta atp11$ and $\Delta atp12$ deletion mutants, respectively, and shown to rescue the respiratory deficient phenotypes. However, neither Atp11p overproduction in *atp2* mutants nor Atp12p overproduction in *atp1* yeast conferred the ability to grow on EG plates at any of the temperatures tested (23°C, 30°C, 37°C) for a period up to one week.

Discussion

The main goal of the research described here was to provide information at the molecular level about mutations in the F₁ α subunit or β subunit that conferred a respiratory deficient

Table 4. Mutations in the α subunit of yeast F₁.

<i>atp1</i> Strain	Amino acid change	Subdomain ^a	Defect
P13	R13K ★ G244E ★	MLS NBD	α and β subunit aggregated
P26	G186D ★	NBD	α and β subunit aggregated
P78	G186D ★	NBD	α and β subunit aggregated
C231	G291D ★	NBD	α and β subunit aggregated
C273	G356R ★	NBD	α and β subunit aggregated
E594	E202K ★	NBD	F ₁ F ₀ dimers(?)
E552	G211D ★	NBD	F ₁ F ₀ dimers(?)
E559	G211D ★	NBD	F ₁ F ₀ dimers(?)
C258	T383I ★	NBD	F ₁ F ₀ dimers(?)
P263	T383I ★	NBD	F ₁ F ₀ dimers(?)
P67	P400S ★	NBD	F ₁ F ₀ dimers(?)
P164	G458D ★	α -helix bundle	F ₁ F ₀ dimers(?)
N112	Q467* ★	α -helix bundle	α and β subunit aggregated
N177	Q478* ★	α -helix bundle	α and β subunit aggregated
E793	D207Y ★	NBD	F ₁ F ₀ multimers

^a β -barrel (N61-I131), NBD (V132-Q416), α -helix bundle (V417-F545)



Fig. 15 Yeast F₁ α _C subunit. 2HLD.pdb chain C rendered as a cartoon with surface shown at 70% transparency. The color scheme is *yellow* for the β -barrel domain, *lime green* for the NBD, and *cyan* for the α -helix bundle. The P-loop (206-GDRQTGKT-213) is colored *black*. AMP-PNP (*red*) is bound in the non-catalytic site.

phenotype to *S. cerevisiae*. There were 12 mutant *atp1* alleles identified in 15 independent isolates of yeast complementation group G50 (Table 4) and 14 *atp2* alleles among 15 strains belonging to complementation group G1 (Table 5). There was no mitochondrial ATPase measured for any of the mutants, except for the *atp2* strain N15 (Tables 2 and 3). Moreover, none of the mutants (including N15) grew on EG plates incubated at the optimal temperature (30°C) for two days. However, there were several *atp1* mutants that exhibited a leaky phenotype on EG plates, which showed evidence of slow growth beginning after 3 days of incubation (discussed below).

The mutations were grouped according to the principal defect they impose on the ATP synthase. Four distinct classes of mutations were distinguished based on the features of the

Table 5. Mutations in the β subunit of yeast F_1 .

<i>atp2</i> Strain	Amino acid change		Subdomain ^a	Defect
N294	A36T G170D	★	β -barrel NBD	α and β subunit aggregated
E618	H57P	★	β -barrel	α and β subunit aggregated
C166	E82L V465M	★	β -barrel α -helix bundle	α and β subunit aggregated
E636	P179L Q408R	★	NBD α -helix bundle	α and β subunit aggregated
E397	R223L	★	NBD	α and β subunit aggregated
E58	G227D	★	NBD	α and β subunit aggregated
E677	G227D	★	NBD	α and β subunit aggregated
E312	P379L	★	NBD	α and β subunit aggregated
N189	Q444Y	★	α -helix bundle	α and β subunit aggregated
N115	S448F	★	α -helix bundle	α and β subunit aggregated
E873	Q412Stop	★	NBD	α and β subunit aggregated
E133	Y482Stop	★	α -helix bundle	α and β subunit aggregated
E323	G323D	★	NBD	α/β dimers
E892	G193D	★	NBD	F_1F_0 multimers
N15	G227D D469N	★	NBD α -helix bundle	Wild type-like assembly, decreased ATP hydrolysis, no ATP synthesis
^a β -barrel (S39-P115), NBD (I116-L391), α -helix bundle (D392-N511)				

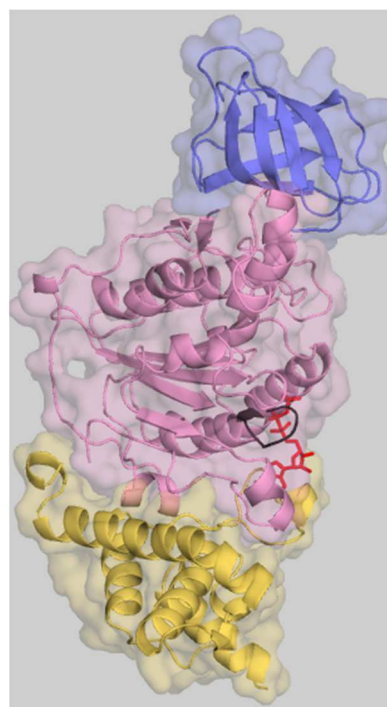


Fig. 16 Yeast $F_1 \beta_D$ subunit. 2HLD.pdb chain D rendered as a cartoon with surface shown at 70% transparency. The color scheme is *slate blue* for the β -barrel domain, *pink* for the NBD, and *yellow-orange* for the α -helix bundle. The P-loon

assembly defects that were observed. Class 1 mutations (*red filled stars*) define mutant proteins that cannot assemble with its partner to form the $\alpha_3\beta_3$ hexamer, leading to aggregation of both the α and β subunits. What is labeled here as a Class 1 assembly defect is the signature phenotype that has been described in detail for $\Delta atp1$ and $\Delta atp2$ deletion strains and for yeast that are deficient for one of the F_1 associated chaperone proteins (e.g. *atp11* or *atp12* mutants).

Approximately one-half of the missense mutations in *ATP1* and most of the missense mutations in *ATP2* were assigned to Class 1 based on the work reported here. Class 2 (*purple filled stars*) were the next most represented mutations, observed in *atp1* mutants harboring the mutations E202K, G211D, T381I, P400S, G458D, and denote cases in which the F_1F_0 structure was assembled, but showed sedimentation properties that suggest it dimerizes in Triton X-100 extracts. Note that two Class 2 mutations (G211D and T381I) were identified in two separate yeast isolates of G50. Class 3 mutations (*green filled stars*) correlate with the assembly of F_1F_0 complexes that oligomerize in Triton X-100 extracts to form multimers that are larger than those observed for Class 2. There was one Class 3 mutation among the members of complementation groups G50 (strain E793) and G1 (strain E892). Remarkably, the *atp1* Class 3 mutation (D207Y) maps to the P-loop in the non-catalytic nucleotide site (NCS) of the α subunit, and the *atp2* Class 3 mutation (G193D) maps to the P-loop in the catalytic site (CS) of the β subunit. The designation Class 4 mutation (*aqua filled star*) was assigned to distinguish the one case (*atp2* strain E323) in which α/β dimers were observed in soluble mitochondrial extracts. Finally, there were two mutations in the *atp2* allele of strain N15 (*red/white star*), one of which (G227D) was shown here (strains E58, E677) and in work published previously (strain N123) (78) to completely prevent F_1 assembly and cause the unassembled F_1 α and β subunits to accumulate as aggregated proteins. The biochemical phenotype of mitochondria from N15 supports the notion

that the 2nd mutation (D469N) can partially suppress the deleterious effect of the G227D mutation. Several of the mutations are described in greater detail in following sections of the discussion.

The 3D models of the α and β subunits (Figures 15 and 16, respectively) shown adjacent to Tables 4 and 5 (and in other figures throughout this section) were made with Pymol® (82) using the coordinates for the 2.8 Å resolution X-ray structure of the yeast F₁ oligomer (2HLD.pdb). Both proteins have nearly identical folds comprised of 3 subdomains, N-terminal b-barrel, C-terminal bundle of α -helices, and nucleotide binding domain (NBD) in between. Figs. 15 and 16 are further annotated to show the position of the P-loops relative to bound nucleotide in the non-catalytic site of α and in the catalytic site of β .

Class 1 assembly defect

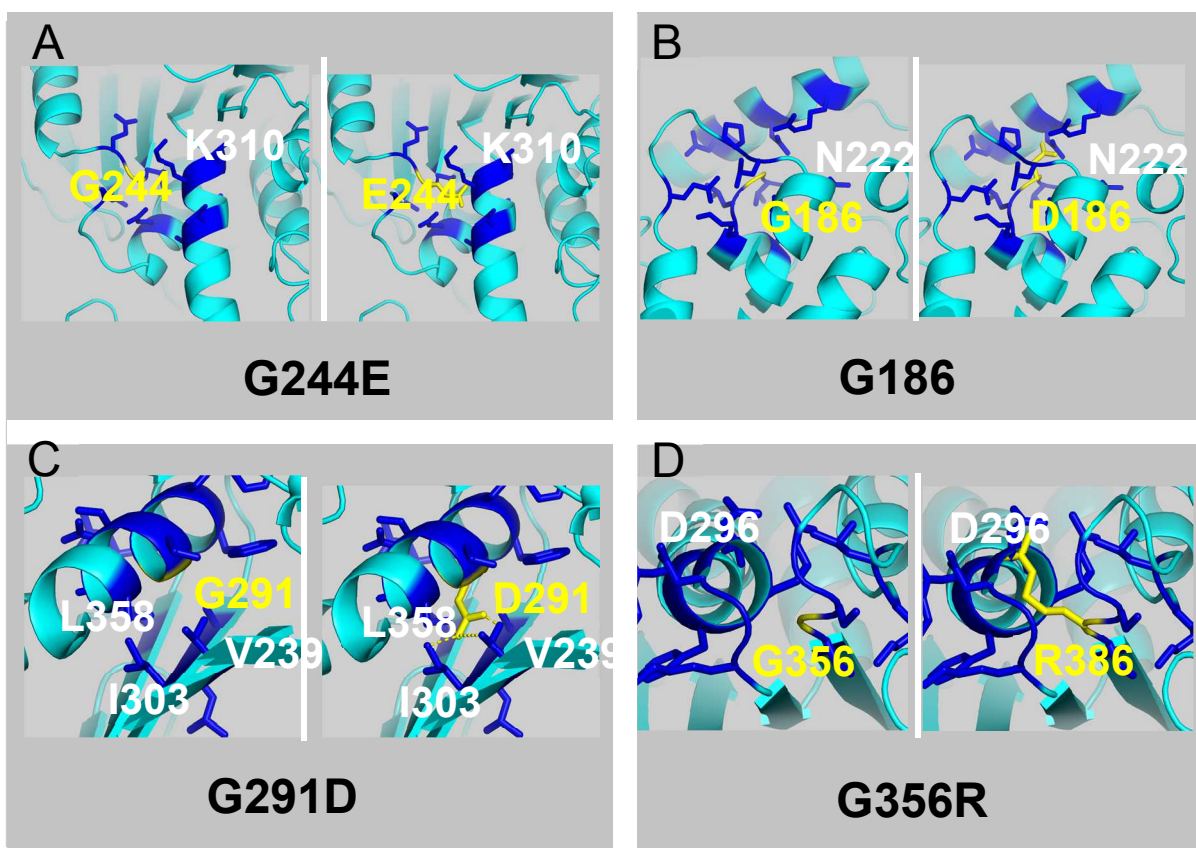


Figure 17. *atp1* mutations correlated with Class 1 assembly defects. The α_c subunit (2HLD.pdb, chain C) was rendered as a cartoon colored cyan. See text for details.

Aggregated F₁ α and β subunits were observed in mitochondria from the yeast that harbor a nonsense mutation in either the *atp1* allele (strains N112, N177, Table 4) or the *atp2* allele (strains E873, E133, Table 5). These mutant genes code for the respective α or β subunit missing part or all of the C-terminal helical domain and will not be discussed further. Four *atp1* missense alleles (G244E, G186D, G291D, and G356R) were shown to encode an α subunit with a Class 1 mutation. The position of the wild type amino acid that is targeted by each of the mutations was located in the α subunit structure (Figure 17, *left-side* of panels *A-D*; lettering and side-chain colored *yellow*). Next, Pymol commands were issued to locate amino acids (colored *blue*) with atoms that were within 4 Å of the substituted amino acid. The pdb files were then modified to replace the wild type with the relevant mutant amino acid (Figure 17, *right-side* of panels *A-D*; lettering and side-chain colored *yellow*). Visual inspection identified, in most cases, only one vicinal amino acid (*white* lettering) that was most likely affected by the substitution in the α subunit. The suggested structural perturbations are due to interference by E244 with K310 in strain P13; by D186 with N222 in strains P26 and P78; by D291 with L358, V239, and/or I303 in strain C231; by R386 with D296 in strain C273. There is a 2nd mutation (R13K) encoded by the *atp1* allele of strain P13 (Table 4). However, it is a conservative substitution in the mitochondrial leader sequence (MLS) that maintains the (+) charge character of the leader peptide and is not expected to be of significant consequence.

Class 2 assembly defect

The Class 2 assembly defect is defined by the association of F₁F₀ in “small” oligomers (possibly dimers) in soluble fractions recovered after mitochondria have been extracted with 0.25% Triton X-100 (Fig. 13). Thus far only *atp1* mutants have been assigned to class 2 (Table 4). An explanation of the effect elicited by the linked mutations in strains E594, E552, E559,

C258, P268, P67, and P164 is complicated by the fact that all of these of these yeast exhibit a leaky respiratory deficient phenotype, which is indicated by all showing growth eventually on YEPG plates. Cumulatively the observations suggest that the mutations in this class exert a relatively modest effect and no further work was done to characterize them further.

Class 3 assembly defect

The Class 3 assembly defect is manifest by F_1F_0 complexes that associate in “large” multimers in soluble fractions recovered after mitochondria have been extracted with 0.25% Triton X-100 (Figs. 11,12). Remarkably, there were two yeast strains identified with this defect, E793 (*atp1* mutation D207Y) and E892 (*atp2* mutation G193D), and in both cases the mutation caused an amino acid substitution in the P-loop that is essential for these proteins to bind nucleotide triphosphates. The glycine-rich P-loop is a conserved primary structure motif that is observed both in proteins that bind ATP, such as adenylate kinase (83), as well as those that bind GTP, including *ras* (84) and the elongation factor *Tu* (85).

The biochemical characteristics of F_1F_0 complexes with the G193D P-loop mutation in the β subunit was found to be very different from that of another *atp2* yeast that makes the mutant protein harboring an A192V substitution in the P-loop (78). In the latter case, the mutation correlates with the assembly of an F_1F_0 with normal physical features, which nonetheless is completely deficient for catalytic activity. Instead, the G193D mutation in the β subunit and the D207Y mutation in the α subunit both alter the F_1F_0 structure in a way that leads to oligomerization of the complexes. It is not known at this time what effect either mutation has on nucleotide binding to the catalytic site (CS) of the β subunit or to the non-catalytic site (NCS) of the α subunit. However, it is important to recall the nucleotide binding cavities are all located at interfaces between α and β subunits in the $\alpha_3\beta_3$ hexamer (Figure 18). It is reasonable to

suggest that either by preventing nucleotide binding or through structural perturbation of the shared sites (or both) might lead to a partial opening of the structure at the interfaces and that this could expose hydrophobic side chains leading to abnormal associations among the F_1F_0 complexes.

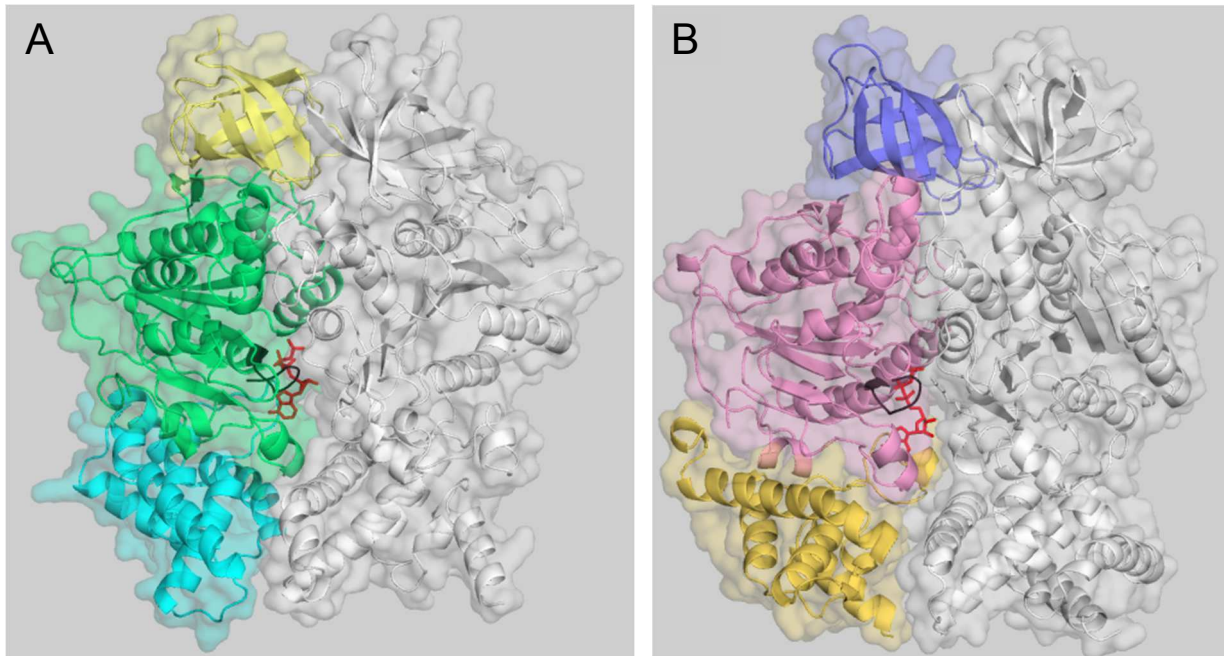


Figure 18. Location of the adenine nucleotide binding sites in F_1 . *A*, Inside view of the NCS in α_C (rendered exactly as shown in Fig. 15, with the P-loop in *black* and bound AMP-PNP in *red*). This NCS is shared with the β_F subunit (2HLD.pdb chain F), which here is rendered as a cartoon in *white* with the surface shown at 70% transparency. *B*, Inside view of the CS in β_D (rendered exactly as shown in Fig. 16 with the P-loop in *black* and bound ADP in *red*). This CS is shared with the α_C subunit., which here is rendered as a cartoon in *white* with the surface shown at 70% transparency.

Class 4 assembly defect

The Class 4 assembly defect was assigned to the *atp2* mutant E323. When mitochondria from this strain were extracted with 0.25% Triton X-100, there was evidence of soluble F_1 α and β (Fig. 7). However, these proteins displayed an abnormal profile when the solubilized material was centrifuged through a 6-20% (Fig. 10), as they were detected at a much lower sucrose

density than the 550 kDa wild type F_1F_0 complex (Fig. 9), or the 360 kDa F_1 oligomer (78), or even lactate dehydrogenase (140 kDa), which was included as a marker protein in the study.

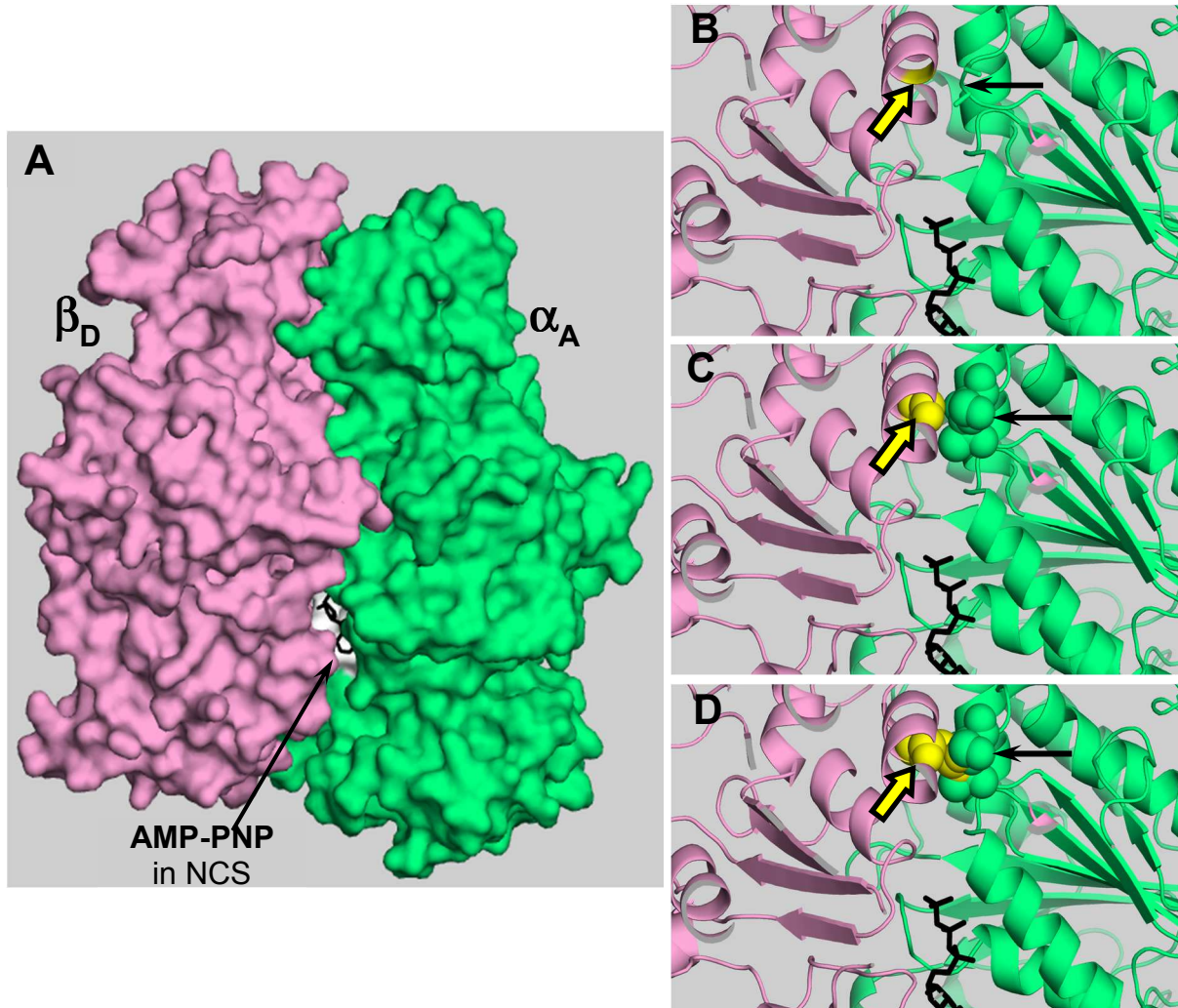


Figure 19. Model of the *atp2* mutation G323D.

A, Outside view of the α_A and the β_D subunits in yeast F_1 (2HLD.pdb, chains A and D, respectively). The β_D and α_A subunits are both rendered as surface-filled molecules. β_D is shaded pink and α_A is shaded lime green except, for the NCS cavity that is white. The *black* arrow points to AMP-PNP (*stick drawing*) in the NCS. *B*, The object in *panel A* was rotated 20° to right, zoomed, and clipped for better visualization of G323 and surrounding amino acids. The F_1 subunits are rendered as cartoons. G323 in β_D is highlighted *yellow* (see also *yellow-filled arrow*). The thick *black* arrow points to a loop in the α_A subunit; the side-chains of A273 and S274 are shown as *sticks*. *C*, Same as *panel B*, except G323 in β_D , and A273 and S274 in the α_A loop are rendered as *spheres*. *D*, Same as *panel C*, except G323 is substituted by *aspartic acid*.

Since the position of the protein peak is consistent with where an $\alpha\beta$ dimer would sediment, the results were interpreted to suggest that the G323D mutation permits the β subunit to assemble with an α subunit, but that F_1 assembly does not proceed beyond that point. G323 is located at the NCS interfaces in F_1 ; for example shown in Fig. 19 between the β_D and α_A subunits in the yeast F_1 structure model. Viewed from outside the F_1 , the AMP-PNP in the NCS is partially visible (Fig. 19, *Panel A*). The view in *panels B-D* was optimized to observe position 323 in the β subunit, which is further up the interface and outside the NCS. *Panels B* and *C* show β -G323 proximal to a loop in the adjacent α subunit that is comprised of α -A273 and α -S274, in which the amino acid residues are either rendered as *sticks* or *spheres*. *Panel D* shows the steric interference that might result when the glycine is replaced by aspartic acid (D323). There was no other point of overlap with D323 in the structure. It remains highly speculative to hypothesize that the structural perturbation modeled in *panel D* could cause the biochemical phenotype observed for the F_1 subunits in strain E323. However, it is extremely interesting to consider the possibility that an intermediate in the F_1 assembly pathway is the $\alpha\beta$ dimer in which the NCS is located.

Model of the F_1 in the *atp2* mutant N15

Four independent isolates of complementation group G1 carry mutant *atp2* alleles that encode the G227D mutation (E58, E677, N15 Table 5; and strain N123 in ref. (78)). This mutation has a severe effect on F_1 assembly in all but strain N15, which bears a second mutation asparagine replacing aspartic acid at position 469 in the β subunit. Though compromised for catalytic activity, the F_1F_0 in N15 mitochondria appears to be assembled correctly (Fig. 14). Figure 20 shows structural models of the β_D subunit of yeast F_1 (*panel A, top*), to explain how

the second-site mutation, D469N, partially suppresses the assembly defect imposed by the G227D primary mutation in yeast strain N15.

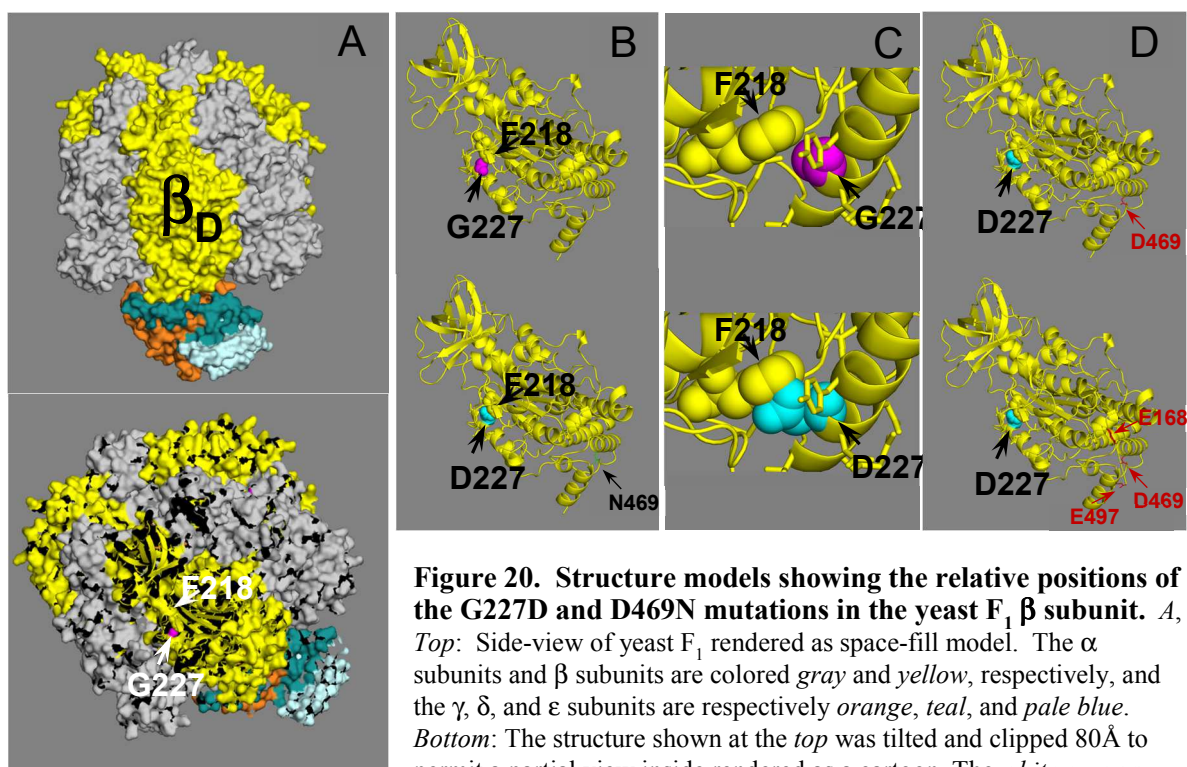


Figure 20. Structure models showing the relative positions of the G227D and D469N mutations in the yeast F_1 β subunit. *A*,

Top: Side-view of yeast F_1 rendered as space-fill model. The α subunits and β subunits are colored *gray* and *yellow*, respectively, and the γ , δ , and ϵ subunits are respectively *orange*, *teal*, and *pale blue*.

Bottom: The structure shown at the *top* was tilted and clipped 80Å to permit a partial view inside rendered as a cartoon. The *white arrows* point to G227

(*magenta* spheres) and F218 (*yellow* spheres). The β_D subunit (labeled) was used to make all of the images shown in panels *B*, *C* and *D*. *Panels B* and *D* show views of the β_D subunit in the same orientation as the *bottom* of *panel A*. *B, Top*: The β_D subunit is shown by itself, rendered as a cartoon, with G227 and F218 annotated in *black*. *Bottom*: The β_D subunit bearing the G227D mutation, with D227 colored *cyan*. The *smaller black arrow* points to N469 (stick rendering), which is the second mutation that was identified in the *atp2* gene cloned from strain N15. *C*, The view of the β_D subunit was rotated and zoomed to show the juxtaposition of F218 versus G227 (*top, magenta spheres*) or D227 (*bottom, cyan spheres*). *D, Top*, Same view of the β_D subunit bearing the G227D mutation as in the *bottom* of *panel B*, with the *red arrow* pointing to D469, which is the wild type amino acid at this position in the yeast β subunit. *Bottom*, same as at the *top* of the panel, with the addition of *two more red arrows* that point to glutamate residues (E168, E497) that are

The proximity of G227 to F218 is shown at the *bottom* of *panel A* and at the *top* of *panels B* and *C*. The position of the two mutations in strain N15 (D227 and N469) are annotated in the structure shown at the *bottom* of *panel B*. *Panel C* is a zoomed view of position 227, in the wild type (G227) at the *top*, and in the mutant (D227) at the *bottom*. There is evidence in the latter that the substitution of aspartic acid for glycine would likely perturb the protein structure due to side-chain overlap with F218. One way to accommodate the crowding would be to rearrange the

protein structure. On this point, the zoomed-out images in *panel D* show the structures of the β subunit bearing only the G227D mutation, pointing out that there is normally an aspartic acid residue at position 469. There are two additional acidic amino acids within 7 Å of D469 (*bottom of panel D*), either of which could impose an ionic barrier to the adjustment in the protein structure that is necessary to counter the G227D mutation. The replacement of D469 with asparagine would avoid such overlap of acidic side chains.

Overexpression of the *ATP11* and *ATP12* genes

Molecular chaperones not only help to restore the native state of the protein during stress conditions but also maintain the activity of protein that is destabilized by a mutation. In the bacteria, *Buchnera*, elevated levels of the GroEL type of chaperone is observed in cells that have higher levels of destabilized proteins due to mutations (86). Laboratory *E.coli* strains that have accumulated multiple deleterious mutations are rescued by an induced overexpression of the chaperones, GroEL or the DnaK (87, 88). Furthermore, overexpression of the chaperone, Hsp70, in fruit flies has suppressed the neurodegeneration caused by proteins with expanded polyglutamine tracts (89). Therefore, it was deemed worthwhile to overproduce the assembly factors Atp12p and Atp11p in the *atp1* and *atp2* mutant strains, respectively, in an attempt to rescue the respiratory defects. Plasmids were constructed with a suitable genetic marker and verified by showing that they each conferred respiratory function to the respective $\Delta atp11$ or $\Delta atp12$ yeast. However, neither the *atp1* nor the *atp2* mutants were rescued by overproduction of Atp12p or Atp11p.

CHAPTER 4: ACCOUNTING FOR POLYMORPHISMS IN THE HUMAN *ATP12* GENE (*ATPAF2*) THAT AFFECTS F₁ BIOGENESIS

Summary

The nuclear gene, *ATP12*, in *S. cerevisiae* encodes a ~36 kDa pre-protein. The first 32 amino acids make up the mitochondrial leader sequence (MLS), which is proteolytically cleaved to generate a ~33 kDa mature protein. This protein is required for the assembly of the F₁ moiety of the mitochondrial ATP synthase. Experiments in yeast has established that the Atp12 is required to assemble the α subunit and absence of Atp12p leads to F₁ aggregated proteins. Using *atp12* yeast mutants, our lab was instrumental in identifying domains important for the functioning of the Atp12p. An important outcome of this study was the identification of an E289K mutation that compromises the function of the Atp12p. A human homolog of the yeast *ATP12* gene was identified as *ATPAF2*. A plasmid bearing the human Atp12p (Atpaf2p) was shown to complement the *atp12* yeast mutant. Furthermore, a substitution from a Glutamate to a Lysine at the corresponding position in the recombinant Atpaf2p had a similar effect as its yeast counterpart.

In 2004 De Meirleir *et. al* reported a W94R mutation in the *ATPAF2* gene that led to the death of a 14-month old. Since the Atpaf2p complements an *atp12* yeast mutant, the yeast model provided an excellent opportunity to study a clinically isolated variant of Atpaf2p. Characterization of the Atpaf2p harboring a W94R mutation revealed that the mutation affects the protein solubility. These observations intrigued us to investigate missense mutations in the SNP database (dbSNP) predicted to be deleterious to a cell, based on amino acid substitution (AAS) models. Our observations led to the identification of two missense mutations, G170V and E241G, that could affect the Atpaf2p activity causing an ATP synthase deficit. The rationale behind choosing these missense mutations are 1) The G170V mutations has low SIFT and

PANTHER scores suggesting greater damage to cells 2) The E241G mutation is adjacent to the E240 residue that is important for functioning of the Atpaf2p. We took advantage of the $\Delta atp12$ yeast model to characterize these missense mutations *in vivo*. The goal of this project was to determine how haplo insufficiency in genes involved in metabolism affects the health of an individual.

Results and discussion

Characterization of yeast strains harboring missense mutations in the *ATPAF2* gene

The yeast plasmid that produces Atpaf2p harboring the E241G and G170 mutations was created by mutagenesis and sub-cloning. The plasmid pG57/ST20 that produces the wild-type Atpaf2p was already available in the laboratory. A 599 bp *XmaI-PstI* containing the entire reading frame of the wild-type *ATPAF2* gene from the *CEN* vector, pRS314, was transferred to a pUC19 vector which was linearized using the same restriction sites. Following the manufacturer's protocol, QuikChange site-directed mutagenesis kit was used with the plasmid pUC19 to induce the G170V and the E241G mutations in the *ATPAF2* gene. The plasmids were sequenced to verify that only the desired mutations were introduced in the reading frame. The *ATPAF2* genes harboring the missense mutations in the pUC19 plasmid were digested with *XmaI-PstI* and purified. These fragments were ligated to the pRS314 *TRP* plasmid using the same restriction sites. Introduction of the plasmids harboring the mutant forms of the *ATPAF2* gene in an $\Delta atp12$ yeast does not rescue the respiratory deficit phenotype as it shows an EG-phenotype. Also, yeast producing the mutant forms of the Atpaf2p show no ATPase activity when compared to yeast producing plasmid encoded wild-type Atpaf2p, suggesting the missense mutations affect its chaperone activity (Table 6).

Table 6. ATPase activities of yeast producing plasmid-borne Atpaf2p.

Strain	Mitochondrial ATPase Activity	
	Minus Oligomycin	Plus Oligomycin
	<i>μmole of NADH consumed/min/mg</i>	
Wild type	3.25 ± 0.89	0.56 ± 0.06
$\Delta atp12p$	0.24 ± 0.12	0.11 ± 0.04
$\Delta atp12p$ + Atpaf2p	1.21 ± 0.21	0.52 ± 0.01
$\Delta atp12p$ + Atpaf2p (E241G)	0.36 ± 0.06	0.17 ± 0.07
$\Delta atp12p$ + Atpaf2p (G170V)	0.27 ± 0.04	0.17 ± 0.04

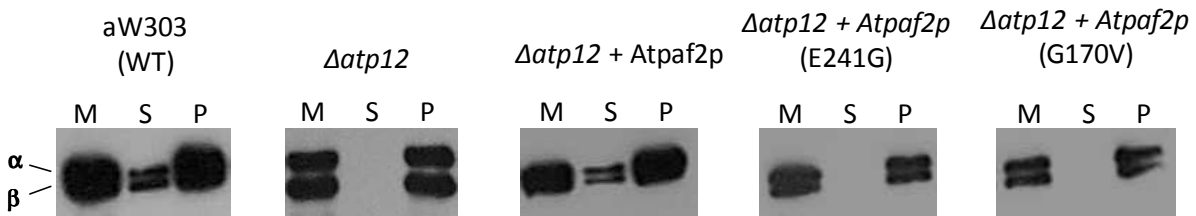


Figure 21. Western analysis showing solubilization of the F₁F_o from yeast mitochondria. Mitochondrial samples prepared from yeast strains shown were extracted with 0.25% TritonX-100 and centrifuged as mentioned under “Materials and Methods”. Aliquots of total mitochondrial protein (*M*) and equivalent volumes of the particulate (*P*) and soluble (*S*) fractions were analyzed by Westerns. The type of *atpaf2* mutation is given in parenthesis.

The mitochondria from strains shown in Fig. 21 were treated with Triton X-100 to evaluate the nature of F₁ defect. The mitochondrial proteins present in the supernatant and particulate fractions were resolved on a SDS-polyacrylamide gel, transferred to nitrocellulose, and probed with antibodies against the F₁ protein to examine its distribution between the fractions. Yeast producing the Atp12p and plasmid encoded Atpaf2p show comparable solubility profiles. This indicates that the wild-type Atpaf2p is active and is capable of assembling the F₁ in a yeast model. However, in the mutant variants of Atpaf2p, all of the F₁ partition in the

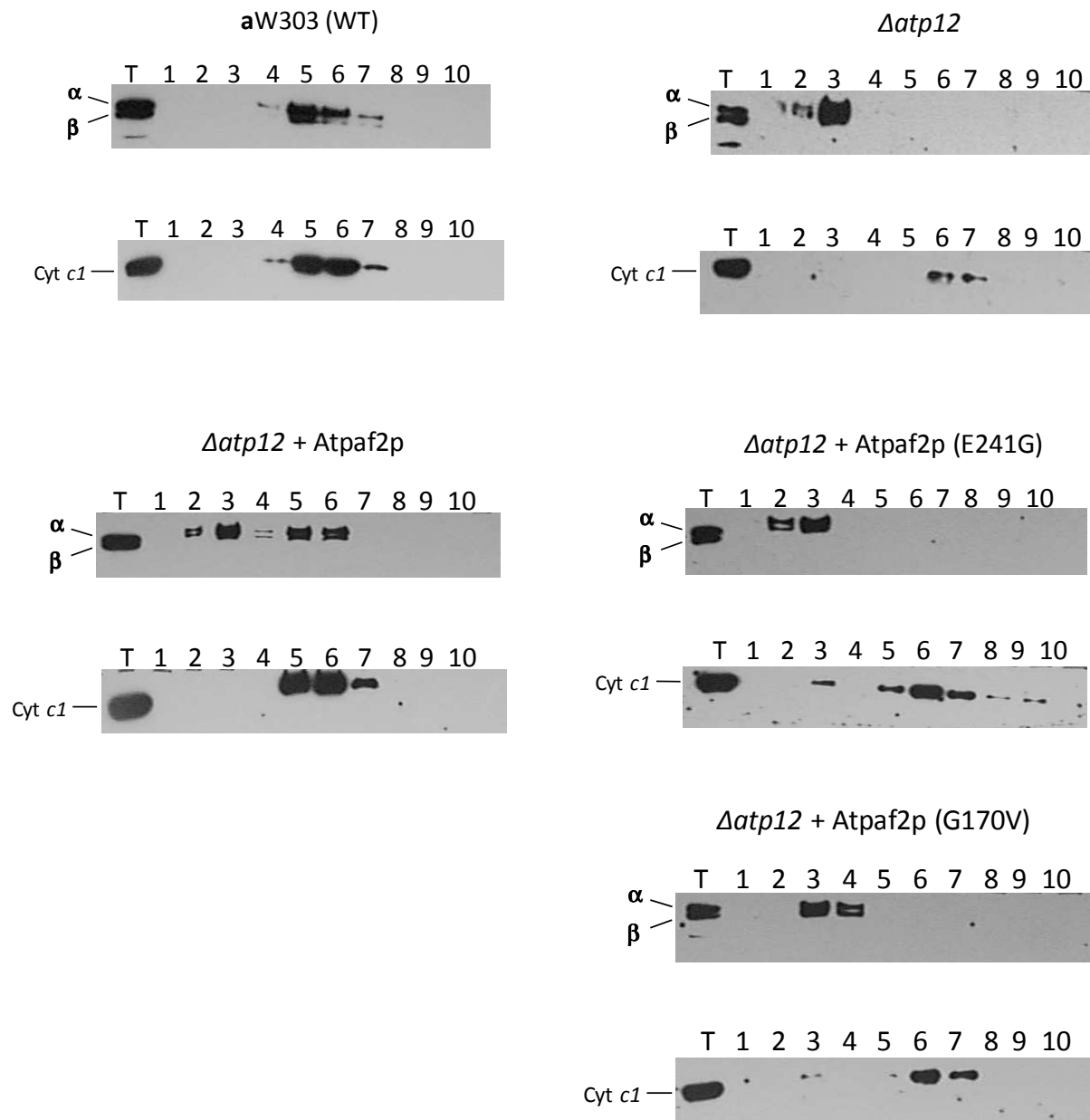


Figure 22. Western analysis of step sucrose gradient fractions. Mitochondria prepared from the wild type strain, aW303, and from mutants, were permeabilized using 0.25% TritonX-100 and centrifuged through 20–80% step sucrose gradients as described under “Materials and Methods.” Ten fractions of equivalent volume were collected from the bottom of the tube, and 15 μ l of each fraction were run on a 12% SDS-polyacrylamide gel. Following transfer to nitrocellulose, the blot was exposed to antibodies against the F₁ α and β subunits and cytochrome *c*₁ (Cyt *c*₁). The positions of the α , β , and Cytochrome *c*₁ protein bands are indicated in the left-hand margin.

particulate fraction. The aggregated F₁ subunits suggests that the missense mutations in Atpaf2p abolishes its activity and is unable to assemble the F₁F₀. This phenotype is similar to F₁ assembly defective yeast that are missing the Atp11p or Atp12p required for F₁ assembly. A step sucrose gradient was performed to investigate if the F₁ is associated with the inner mitochondrial membrane. The yeast capable of producing the wild-type Atpaf2p shows two peaks for the F₁ protein. One peak is at the 50-60% sucrose interface and co-migrates with cytochrome *c*₁, indicating that the F₁F₀ is membrane bound. The second peak is observed at the 60-80% interface indicative of higher molecular weight aggregates (Fig. 22). This observation suggests that the Atpaf2p is capable of assembling F₁F₀ in an Δ *atp12* yeast but may not be efficient as its yeast counterpart (Fig 22). A similar analysis performed with yeast producing missense mutations in the Atpaf2p show aggregated F₁ in the 80% sucrose fraction recapitulating an assembly defective phenotype.

The goal of this project was to evaluate the effect of missense mutations in the Atpaf2p genes from the SNP database. We identified two missense mutations, G170V and E241G, that were of interest and observe that these mutations affect the activity of the Atpaf2p producing an F₁ assembly defect.

CHAPTER 5: THE N-TERMINAL DOMAINS OF ATP11P

Summary

The nuclear gene (*ATP11*) for *S. cerevisiae* Atp11p encodes a ~39 kDa pre-protein with 318 amino acids. The first 39 residues encompass the mitochondrial leader sequence (MLS), which when removed generates a ~32 kDa (Fig. 23, *panels A and B*) (90). Work published 20 years ago (91) disclosed the sequence between D112 and A300 to be the minimal boundary of the functional domain of yeast Atp11p (Fig. 23, *B*).

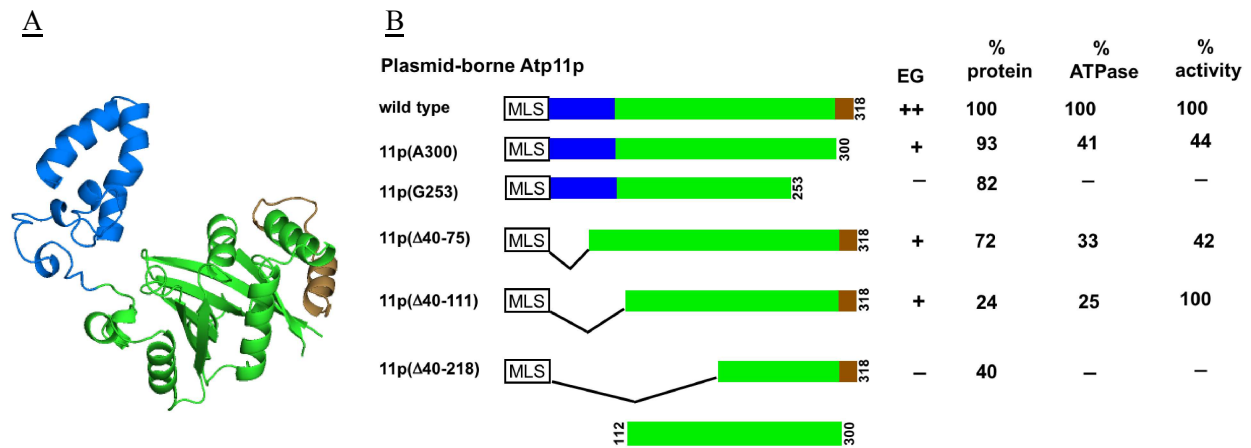


Figure 23. Structure and domains of Atp11p. (A) The cartoon in the figure indicates the different domains in the Atp11p (B) Variants of Atp11p that are encoded by a plasmid. Yeast strains producing the deleted forms of Atp11p were evaluated for its respiratory growth properties, proteins levels, and ATP synthase activities.

In brief, $\Delta atp11$ yeast were transformed with plasmids bearing partial fragments of Atp11p and evaluated for growth on EG plates. Next, mitochondria were prepared from each transformant and analyzed by Western for Atp11p and by enzyme assay for oligomycin-sensitive ATPase activity. Finally, based on the assumptions that the level of ATP synthase activity reflected the level of assembled enzyme and that this value correlated with the amount of Atp11p in mitochondria, the activity retained by each truncated protein, relative to wild type, was estimated by dividing the percent ATPase activity by the percent of immuno-detectable Atp11p. The most interesting observation from this work was obtained with the 11p Δ 40-111

transformant, which showed that the region extending from E40 and L111 could be removed from Atp11p with essentially no impact on the protein activity (Fig. 23 B); i.e. the amount of assembled F₁ correlated well with the amount of the 23 kDa Atp11p variant in mitochondria. These results identified the first 72 amino acids of mature Atp11p (post import/processing) as a separate domain at the N-terminus of the protein (Fig. 23, colored *blue*).

Interest in the N-terminal domain (NTD) of Atp11p was heightened by fortuitous observations made by members of the laboratory who were trying to determine the protein structure at atomic resolution. Initial work was done using recombinant Atp11p (Rc11p) comprised of the sequence extending from E40 to N318, which mimicked the mature, mitochondrial form of the protein (90). Highly purified preparations of *S. cerevisiae* Rc11p failed to crystallize and the ¹⁵N,²H-labeled recombinant protein produced a poorly resolved 2-D nuclear magnetic resonance (NMR) spectrum, typical of proteins not stably residing in a single conformation. Remarkably, the NMR data improved dramatically with a form of Rc11p that was cleaved *in vitro* to remove the NTD (92). In a similar vein, while the full-length RcAtp11p from *Candida glabrata* eventually afforded well-diffracting protein crystals, the NTD is missing from the high resolution X-ray structure (93), which includes only the *green* and *brown shaded* regions of the cartoon rendering shown in panel A of Fig. 23. The *blue* helix was modeled using the Scratch Protein Predictor at <http://scratch.proteomics.ics.uci.edu/>. (94) to analyze the NTD amino acid sequence of *C. glabrata* Atp11p.

Cumulatively, the information about the NTD of Atp11p suggested it might be a member of a recently-recognized protein class that is distinguished on the basis of intrinsic disorder (95). The high intra-molecular flexibility of intrinsically disordered polypeptide domains imposes unique functional properties with respect to well-ordered proteins. If, in fact, the NTD of

Atp11p was not required to support assembly of F₁ *in vivo*, perhaps it served a regulatory purpose. However, before embarking on a full-scale investigation of this hypothesis, it was deemed important to first clarify a point of uncertainty with respect to how the data for the 11p Δ 40-75 and 11p Δ 40-111 yeast transformants (Fig. 23, B) was interpreted (96). The level of activity attributed to the N-terminally deleted variants of Atp11p produced in these yeast assumed that the relative amount of the protein detected in Western blots reflected how much protein was actually produced from the plasmids (see above). This was a valid assumption provided that the antigenic determinants for the polyclonal antibody raised against Rc11p are distributed evenly along the primary amino acid sequence. If, on the other hand, the majority of antigenic sites are clustered in the NTD, the amount of a protein from which a part (Δ 40-75) or all (Δ 40-111) of this sequence was missing would be underestimated by Western analysis. An affinity tag fused to the C-terminus of the N-terminally truncated Atp11p proteins would enable its amount in protein blots to be measured using a read-out that was independent of Atp11p features. Based on the success in previous work (97) that employed avidin conjugates to detect a biotinylated Atp11p-carboxylase fusion protein in mitochondria (abbreviated here as Bt11p), the plasmid to produce 11p(Δ 40-75) was re-engineered to include an in-frame fusion at the 3' end of the gene to the DNA coding for a peptide that gets biotinylated in yeast. Studies were then pursued with yeast transformants that produced either Bt11p or Bt11p(Δ 40-75).

Results and Discussion

Characterization of yeast strain producing biotinylated Atp11p

The yeast vector to produce Bt11p(Δ 40-75) was created by sub-cloning fragments from plasmids that were already available in the laboratory. One of them, pG13/ST16, directs the production of Bt11p from a gene fusion between yeast *ATP11* and the DNA coding for the biotin

attachment peptidyl region of a transcarboxylase enzyme from *Priopiobacterium shermanii* (97). The other, pBSE, carries the modified gene used to produce 11p(Δ 40-75), (91). First, a 1427 bp *SacI-HindIII* fragment from the 2μ plasmid pG13/ST16 was transferred to a *CEN* vector, pRS316 (98), which had been linearized using the same restriction enzymes. The intermediate plasmid was digested with *SacI* and *NcoI*, which removed the codons for Bt11p up to the *NcoI* site near the 3' end of the gene. The larger of the two generated fragments was purified and ligated with a 973 bp *SacI-NcoI* fragment from pBSE, which replaced the wild type *ATP11* sequence, upstream from the internal *NcoI* site, with the DNA coding for the Δ 40-75 deletion and generated a single copy *URA3* plasmid. The introduction of this plasmid in Δ *atp11* yeast partially rescued the respiratory defect as judged by the change from an EG- to a slow EG+ phenotype. However, there was no oligomycin-sensitive ATPase activity detected in mitochondria purified from the transformant (Table 7). Also the percentage of ATP synthase that partitioned to the soluble fraction following Triton X-100 treatment of mitochondria was less in samples from yeast that produce Bt11p(Δ 40-75) versus the transformant that makes regular 11p(Δ 40-75) from a plasmid (Fig. 24).

Table 7. ATPase activities of yeast producing plasmid-borne Atp11p variants.

Strain	ATPase activity	
	Minus Oligomycin	Plus Oligomycin
	<i>μmole of NADH consumed/min/mg</i>	
Atp11p	1.32 ± 0.02	0.26 ± 0.04
Δ <i>atp11p</i>	0.29 ± 0.11	0.16 ± 0.02
11p(Δ 40-75)	0.40 ± 0.03	0.20 ± 0.02
Bt11p	1.62 ± 0.16	0.40 ± 0.03
Bt11p(Δ 40-75)	0.20 ± 0.03	0.12 ± 0.02

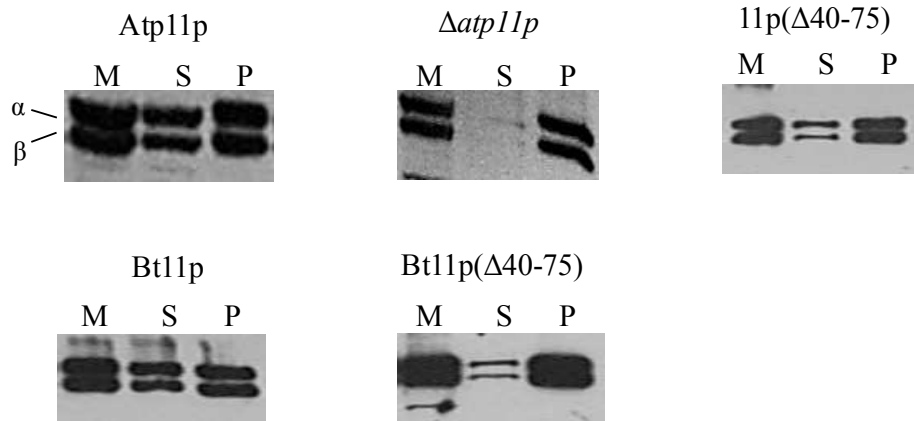


Figure 24. Western analysis showing F₁F₀ extraction from yeast producing Atp11p from plasmids. Mitochondrial samples prepared from yeast strains shown were extracted with 0.25% TritonX-100 and centrifuged as mentioned under “Materials and Methods”. Aliquots of total mitochondrial protein (*M*) and equivalent volumes of the particulate (*P*) and soluble (*S*) fractions were analyzed by Westerns.

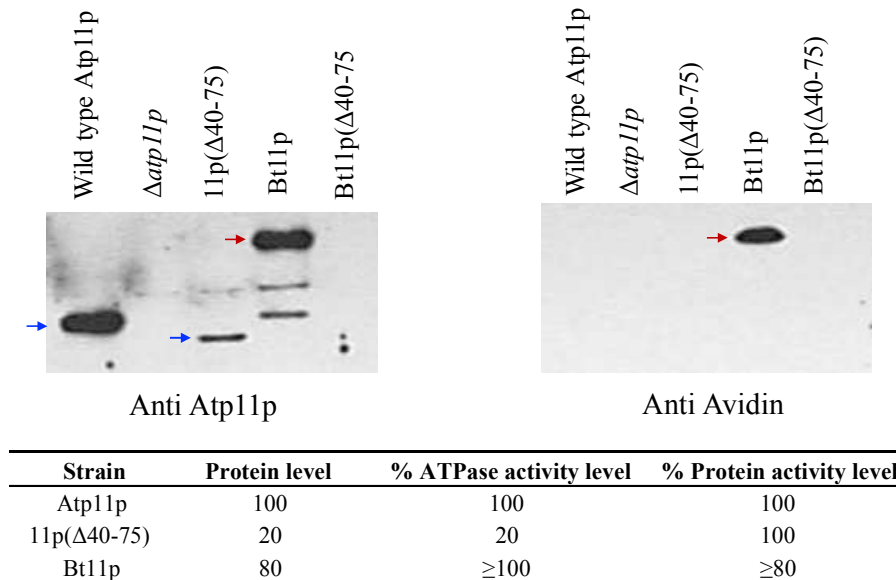


Figure 25. Protein blots of mitochondria from yeast transformants that produce Atp11p proteins from plasmids. *Upper*, mitochondria were prepared from non-transformed $\Delta atp11$ and the transformants that carried the relevant plasmid to produce the various Atp11p proteins indicated in the figure. Equivalent amounts of total mitochondrial protein (20 μ g) were loaded in each lane of a 12% SDS-polyacrylamide gel. Gel separation and transfer to nitrocellulose were done as described in “Materials and Methods”. Each of the samples were probed with Anti-Atp11p to quantify how much Atp11p was present, and with and HRP-Avidin to determine if the biotin tag was present. *Lower*, the Western signals for Atp11p were quantified by densitometry to determine the % vs. wild type, and the latter values were divided by the % oligomycin-sensitive ATPase activity detected to estimate the activity of the proteins.

The mitochondria from the 5 strains shown in Table 7 and Fig. 24 were also evaluated for the level of Atp11p. The mitochondrial proteins were resolved in SDS-polyacrylamide gels, transferred to nitrocellulose, and the blots were treated with polyclonal anti-Atp11p serum or horse-radish peroxidase (HRP) conjugated avidin (Fig. 25). The Western blot showed immune-reactive full-length Atp11p and 11p(Δ 40-75) proteins (*blue arrows*) of the expected sizes and Bt11p was detected with both the antibody and HRP-avidin (*red arrows*). However, there was no Bt11p(Δ 40-75) picked up with either probe. A densitometry analysis was performed using the Kodak 1D imaging system to determine the relative amounts of the proteins that were detected by Western, and these values were used in combination with the oligomycin-sensitive ATPase activities in each sample to estimate the level of Atp11p as described above for Fig. 23. Whereas a similar analysis performed previously had indicated 11p(Δ 40-75) was only 46% active (Fig. 23), the more recent results showed that the transformed yeast produced 20% the wild type level of 11p(Δ 40-75) protein, and this correlated with ~20% oligomycin-sensitive ATPase, which suggests the non-biotinylated truncated protein is, in fact, fully active.

The goal of these experiments was to examine the amount of 11p(Δ 40-75) relative to wild type in mitochondria in a manner that was independent of its physical characteristics. We conclude that combining a C-terminal biotinylation sequence with the Δ 40-75 deletion dramatically reduces the stability of the protein and made it impossible to detect Bt11p(Δ 40-75). No further work targeting the NTD of Atp11p was pursued.

CHAPTER 6: SCOPE OF THE STUDY AND LIMITATIONS

The ATP synthase is a multimeric enzyme that consists of nineteen different polypeptides. Broadly the ATP synthase is divided into three separate structures. 1) An F_0 region that is embedded in the mitochondrial matrix. 2) A hydrophilic F_1 region that is facing the mitochondrial matrix. 3) A peripheral stalk or “stator” area that connects helps connect the F_1 to the F_0 . Our laboratory has always been interested in the assembly of the mitochondrial F_1 -ATPase and therefore more emphasis will be given to it. The F_1 subunit of the mitochondrial ATP synthase consists of α_3 , β_3 , γ , δ , and ϵ . The F_1 subunits are encoded by the nucleus and are imported into the mitochondrial matrix for the assembly of the F_1 . Many of these subunits were identified by chemical mutagenesis of wild-type yeast, D273, and selected for respiratory growth defect on a non-fermentable source such as ethanol-glycerol medium. The α and β subunits form an alternating structure with the subunits containing the nucleotide binding domains that become catalytically active when there is a contribution from the neighboring subunits. The absence of either the α or β the subunits results in the aggregation of the corresponding subunits as insoluble proteins in the mitochondrial matrix. A similar effect is observed with yeast strains lacking the assembly factors for the α and β subunits, *Atp12p* and *Atp11p* respectively.

Mutagenesis of wild-type yeast led to the identification of independent isolates harboring mutations in the F_1 α (G50) or β subunit (G1). Studies with six of the 22 *atp2* mutants by our laboratory have shown that mutations in the β subunit affect the activity of the ATP synthase or is assembly defective. The aim of this thesis was to study the biochemistry of the ATP synthase in the remainder of the *atp2* mutants and all of the *atp1* mutants. Our studies reveal "novel" phenotypic characteristics in the *atp1* and *atp2* mutants that have not been observed or reported previously. The *atp2* mutant, N15, shows 40% wild-type levels of enzyme activity and presence

of an assembled F_1F_0 . This mutant harbors two mutations in the reading frame of the *atp2* gene (G227D, D469N). It has been observed that yeast isolates harboring only the G227D are defective for the enzyme assembly. Therefore, it suggests that the D469N mutation suppresses the effects of the G227D mutation. We have explained this suppressor effect using a structural model as described in the "Discussion" section. However, molecular dynamics simulation and site-directed mutagenesis will provide greater insight into the phenotypic characteristic of the *atp2* mutant N15.

Two yeast mutants that showed similar biochemical properties were E793 (*atp1*) and E892 (*atp2*). These mutants show no enzyme activity but demonstrate the presence of soluble α and β subunits. Using linear sucrose gradients, we observed that these mutants produce large oligomers of the F_1F_0 . Surprisingly each of these mutations maps to the P-loop region of the alpha and beta subunits. Study in our laboratory of an *atp2* mutant (A192V) with a P-loop mutation shows a solubility profile similar to the wild-type yeast with the loss of an enzyme activity and therefore this result was unexpected. At present, we are unable to explain satisfactorily why these yeast mutants form higher order oligomers of F_1F_0 when extracted from the membrane using a detergent. We suggest that these P-loop mutations expose certain hydrophobic surfaces within the nucleotide binding regions causing it to oligomerize. It would be interesting to investigate whether the oligomerization phenomenon is unique to individual amino acids in the P-loop region.

Another novel phenotype that we observed was in the *atp2* mutant E323. This mutant yeast produces $\alpha\beta$ dimers but is incapable of F_1 assembly. We have not been able to ascertain at what point during assembly the process is hindered. Immuno co-precipitation will allow us to identify if other subunits of the F_1 are associated with the $\alpha\beta$ dimers.

Our study opens new avenues in understanding the structure and the mechanism of the ATP synthase. Although similar work has been carried out with the bacterial ATP synthase in various domains, it is not an ideal system because the yeast mitochondrial ATP synthase shares structural and functional homology with the human ATP synthase. Mutational studies allow us to observe how the biochemistry of the ATP synthase is affected. With polymorphisms found in different human populations, one can predict if a missense mutation has an effect on the structure or the activity of the enzyme. It also allows us to identify if a mutation in the ATP synthase has a pleiotropic effect on other respiratory chain proteins or other mitochondrial proteins.

REFERENCES

1. Ephrussi, S. (1955) © 1955 Nature Publishing Group
2. Corneo, G., Moore, C., Sanadi, D. R., Grossman, L. I., and Marmur, J. (1966) Mitochondrial DNA in yeast and some mammalian species. *Science*. **151**, 687–689
3. Tzagoloff, a, and Dieckmann, C. L. (1990) *PET* genes of *Saccharomyces cerevisiae*. *Microbiol. Rev.* **54**, 211–225
4. Steinmetz, L. M., Scharfe, C., Deutschbauer, A. M., Mokranjac, D., Herman, Z. S., Jones, T., Chu, A. M., Giaever, G., Prokisch, H., Oefner, P. J., and Davis, R. W. (2002) Systematic screen for human disease genes in yeast. *Nat Genet.* **31**, 400–404
5. Prokisch, H., Scharfe, C., Camp, D. G., Xiao, W., David, L., Andreoli, C., Monroe, M. E., Moore, R. J., Gritsenko, M. A., Kozany, C., Hixson, K. K., Mottaz, H. M., Zischka, H., Ueffing, M., Herman, Z. S., Davis, R. W., Meitinger, T., Oefner, P. J., Smith, R. D., and Steinmetz, L. M. (2004) Integrative analysis of the mitochondrial proteome in yeast. *PLoS Biol.* 10.1371/journal.pbio.0020160
6. Reinders, J., Zahedi, R. P., Pfanner, N., Meisinger, C., and Sickmann, A. (2006) Toward the complete yeast mitochondrial proteome: Multidimensional separation techniques for mitochondrial proteomics. *J. Proteome Res.* **5**, 1543–1554
7. Pagliarini, D. J., Calvo, S. E., Chang, B., Sheth, S. A., Vafai, S. B., Ong, S. E., Walford, G. A., Sugiana, C., Boneh, A., Chen, W. K., Hill, D. E., Vidal, M., Evans, J. G., Thorburn, D. R., Carr, S. A., and Mootha, V. K. (2008) A Mitochondrial Protein Compendium Elucidates Complex I Disease Biology. *Cell*. **134**, 112–123
8. Tuppen, H. A. L., Blakely, E. L., Turnbull, D. M., and Taylor, R. W. (2010) Mitochondrial DNA mutations and human disease. *Biochim. Biophys. Acta.* **1797**, 113–28

9. Yoon, Y. G., Koob, M. D., and Yoo, Y. H. (2010) Re-engineering the mitochondrial genomes in mammalian cells. *Anat. Cell Biol.* **43**, 97–109
10. Lasserre, J.-P., Dautant, A., Aiyar, R. S., Kucharczyk, R., Glatigny, A., Tribouillard-Tanvier, D., Rytka, J., Blondel, M., Skoczen, N., Reynier, P., Pitayu, L., Rotig, A., Delahodde, A., Steinmetz, L. M., Dujardin, G., Procaccio, V., and di Rago, J.-P. (2015) Yeast as a system for modeling mitochondrial disease mechanisms and discovering therapies. *Dis. Model. Mech.* **8**, 509–526
11. Fox, T., and Bonnefoy, N. (2007) Directed alteration of *Saccharomyces cerevisiae* mitochondrial DNA by biolistic transformation and homologous recombination. *Methods Mol. Biol.* **372**, 153–166
12. Meunier, B., Fisher, N., Ransac, S., Mazat, J., and Brasseur, G. (2013) Biochimica et Biophysica Acta Respiratory complex III dysfunction in humans and the use of yeast as a model organism to study mitochondrial myopathy and associated diseases. *BBA - Bioenerg.* **1827**, 1346–1361
13. Besagni, L., Luca, C. D. E., Morea, V., Oliva, R., Montanari, A., Tramontano, A., Bolotin-fukuhara, M., Frontali, L., and Francisci, S. (2008) Yeast as a model of human mitochondrial tRNA base substitutions : Investigation of the molecular basis of respiratory defects. **69**, 275–283
14. Magdalena, A., Lasserre, J., Ackerman, S. H., Rago, J., and Kucharczyk, R. (2014) Biochimie De fi ning the impact on yeast ATP synthase of two pathogenic human mitochondrial DNA mutations , T9185C and T9191C. *Biochimie.* **100**, 200–206
15. Bourgeron, T., Rustin, P., Chretien, D., Birch-Machin, M., Bourgeois, M., Viegas-Péquignot, E., Munnich, A., and Rötig, A. (1995) Mutation of a nuclear succinate

- dehydrogenase gene results in mitochondrial respiratory chain deficiency. *Nat. Genet.* **11**, 144–149
16. Calvo, S. E., Tucker, E. J., Compton, A. G., Kirby, D. M., Crawford, G., Burt, N. P., Rivas, M., Guiducci, C., Bruno, D. L., Goldberger, O. A., Redman, M. C., Wiltshire, E., Wilson, C. J., Altshuler, D., Gabriel, S. B., Daly, M. J., Thorburn, D. R., and Mootha, V. K. (2010) High-throughput, pooled sequencing identifies mutations in *NUBPL* and *FOXRED1* in human complex I deficiency. *Nat. Genet.* **42**, 851–858
 17. Werner, K. J. H., Willems, P. H. G. ., and Smeitink, J. A. (2012) Monogenic Mitochondrial Disorders. *N. Engl. J. Med.* **366**, 1132–1141
 18. Rhee, H., Zou, P., Udeshi, N. D., Martell, J. D., and Mootha, V. K. (2013) Proteomic Mapping of Mitochondria. *Science.* **339**, 1328–1131
 19. Abrahams, J. P., Leslie, A. G., Lutter, R., and Walker, J. E. (1994) Structure at 2.8 Å resolution of F₁-ATPase from bovine heart mitochondria. *Nature.* **370**, 621–628
 20. Jiang, W., Hermolin, J., and Fillingame, R. H. (2001) The preferred stoichiometry of *c* subunits in the rotary motor sector of Escherichia coli ATP synthase is 10. *Proc. Natl. Acad. Sci. U. S. A.* **98**, 4966–71
 21. Ballhausen, B., Altendorf, K., and Gabriele, D. H. (2009) Constant *c10* Ring Stoichiometry in the Escherichia coli ATP Synthase Analyzed by Cross-Linking. *J. Bacteriol.* **191**, 2400–2404
 22. Stock, D., Leslie, A. G., and Walker, J. E. (1999) Molecular architecture of the rotary motor in ATP synthase. *Science.* **286**, 1700–5
 23. Stahlberg, H., Müller, D. J., Suda, K., Fotiadis, D., Engel, A., Meier, T., Matthey, U., and Dimroth, P. (2001) Bacterial Na⁺-ATP synthase has an undecameric rotor. *EMBO Rep.* **2**,

229–233

24. Meyer Zu Tittingdorf, J. M. W., Rexroth, S., Schäfer, E., Schlichting, R., Giersch, C., Dencher, N. A., and Seelert, H. (2004) The stoichiometry of the chloroplast ATP synthase oligomer III in *Chlamydomonas reinhardtii* is not affected by the metabolic state. *Biochim. Biophys. Acta - Bioenerg.* **1659**, 92–99
25. Balakrishna, A. M., Seelert, H., Marx, S.-H., Dencher, N. a, and Grüber, G. (2014) Crystallographic structure of the turbine *c*-ring from spinach chloroplast F₁-ATP synthase. *Biosci. Rep.* 10.1042/BSR20130114
26. Pogoryelov, D., Yu, J., Meier, T., Vonck, J., Dimroth, P., and Muller, D. J. (2005) The *c15* ring of the *Spirulina platensis* F-ATP synthase: F₁/F₀ symmetry mismatch is not obligatory. *EMBO Rep.* **6**, 1040–1044
27. Ackerman, S. H., and Tzagoloff, A. (1990) Identification of two nuclear genes (*ATP11*, *ATP12*) required for assembly of the yeast F₁-ATPase. *Proc. Natl. Acad. Sci. U. S. A.* **87**, 4986–90
28. Wang, Z. G., and Ackerman, S. H. (2000) The assembly factor Atp11p binds to the β subunit of the mitochondrial F₁-ATPase. *J. Biol. Chem.* **275**, 5767–5772
29. Wang, Z. G., Sheluho, D., Gatti, D. L., and Ackerman, S. H. (2000) The α subunit of the mitochondrial F₁-ATPase interacts directly with the assembly factor Atp12p. *EMBO J.* **19**, 1486–93
30. Ackerman, S. H. (2002) Atp11p and Atp12p are chaperones for F₁-ATPase biogenesis in mitochondria. *Biochim. Biophys. Acta - Bioenerg.* **1555**, 101–105
31. Lefebvre-legendre, L., Vaillier, J., Benabdelhak, H., Velours, J., Slonimski, P. P., Rago, J., and Se, V. (2001) Identification of a Nuclear Gene (*FMCI*) Required for the Assembly

- / Stability of Yeast Mitochondrial F₁ -ATPase in Heat Stress Conditions. *J. Biol. Chem.* **276**, 6789–6796
32. Francis, B. R., and Thorsness, P. E. (2011) Mitochondrion Hsp90 and mitochondrial proteases *Yme1* and *Yta10/12* participate in ATP synthase assembly in *Saccharomyces cerevisiae*. *MITOCH.* **11**, 587–600
 33. Rak, M., Gokova, S., and Tzagoloff, A. (2011) Modular assembly of yeast mitochondrial ATP synthase. *EMBO J.* **30**, 920–930
 34. Watt, I. N., Montgomery, M. G., Runswick, M. J., Leslie, A. G. W., and Walker, J. E. (2010) Bioenergetic cost of making an adenosine triphosphate molecule in animal mitochondria. *Proc. Natl. Acad. Sci. U. S. A.* **107**, 16823–16827
 35. Lytovchenko, O., Naumenko, N., Oeljeklaus, S., Schmidt, B., Der, K. Von, Deckers, M., Warscheid, B., Laan, M. Van Der, and Rehling, P. (2014) The INA complex facilitates assembly of the peripheral stalk of the mitochondrial F₁F₀ -ATP synthase. **33**, 1624–1638
 36. Seelert, H., and Dencher, N. A. (2011) ATP synthase superassemblies in animals and plants: Two or more are better. *Biochim. Biophys. Acta - Bioenerg.* **1807**, 1185–1197
 37. Paumard, P., Vaillier, J., Coulary, B., Schaeffer, J., Soubannier, V., Mueller, D. M., Brèthes, D., Di Rago, J. P., and Velours, J. (2002) The ATP synthase is involved in generating mitochondrial cristae morphology. *EMBO J.* **21**, 221–230
 38. Schägger, H., and Pfeiffer, K. (2000) Supercomplexes in the respiratory chains of yeast and mammalian mitochondria. *EMBO J.* **19**, 1777–1783
 39. Soubannier, V., Vaillier, J., Paumard, P., Coulary, B., Schaeffer, J., and Velours, J. (2002) In the absence of the first membrane-spanning segment of subunit 4(b), the yeast ATP synthase is functional but does not dimerize or oligomerize. *J. Biol. Chem.* **277**, 10739–

10745

40. Davies, K. M., Anselmi, C., Wittig, I., Faraldo-gómez, J. D., and Kühlbrandt, W. (2012) Structure of the yeast F₁F₀-ATP synthase dimer and its role in shaping the mitochondrial cristae. *Proc. Natl. Acad. Sci.* **109**, 13602–13607
41. Penefsky, H. S., Penefsky, H. S., Company, A. P., and Company, A. P. (1982) Mechanism of ATP Hydrolysis by Beef Heart Mitochondrial ATPase. *Biol. Chem.* **257**, 12092–12100
42. Grubmeyer, C., and Penefsky, H. S. (1981) The presence of two hydrolytic sites on beef heart mitochondrial adenosine triphosphatase. *J. Biol. Chem.* **256**, 3718–3727
43. Gresser, M. J., Myers, J. A., and Boyer, P. D. (1982) Catalytic site cooperativity of beef heart mitochondrial F₁ adenosine triphosphatase. Correlations of initial velocity, bound intermediate, and oxygen exchange measurements with an alternating three-site model. *J. Biol. Chem.* **257**, 12030–12038
44. Rodenburg, R. J. T. (2011) Biochemical diagnosis of mitochondrial disorders. *J. Inherit. Metab. Dis.* **34**, 283–292
45. Lieber, D. S., Calvo, S. E., Shanahan, K., Slate, N. G., Liu, S., Hershman, S. G., Gold, N. B., Chapman, B. A., Thorburn, D. R., Berry, G. T., Schmahmann, J. D., Borowsky, M. L., Mueller, D. M., Sims, K. B., and Mootha, V. K. (2013) Targeted exome sequencing of suspected mitochondrial disorders. *Neurology.* **80**, 1762–1770
46. Jonckheere, A. I., Herma Renkema, G., Bras, M., Van Den Heuvel, L. P., Hoischen, A., Gilissen, C., Nabuurs, S. B., Huynen, M. A., De Vries, M. C., Smeitink, J. A. M., and Rodenburg, R. J. T. (2013) A complex V *ATP5A1* defect causes fatal neonatal mitochondrial encephalopathy. *Brain.* **136**, 1544–1554
47. Holt, I. J., Harding, a E., Petty, R. K., and Morgan-Hughes, J. a (1990) A new

- mitochondrial disease associated with mitochondrial DNA heteroplasmy. *Am. J. Hum. Genet.* **46**, 428–33
48. Robinson, B. H., and Tatuch, Y. (1994) The Mitochondrial DNA Mutation At 8993 Associated With NARP Slows The Rate Of ATP Synthesis In Isolated Lymphoblast Mitochondria. *Biochem. Biophys. Res. Commun.* **192**, 124–128
49. Baracca, A., Barogi, S., Carelli, V., Lenaz, G., and Solaini, G. (2000) Catalytic activities of mitochondrial ATP synthase in patients with mitochondrial DNA T8993G mutation in the ATPase 6 gene encoding subunit *a*. *J. Biol. Chem.* **275**, 4177–4182
50. Trounce, I., Neill, S., and Wallace, D. C. (1994) Cytoplasmic transfer of the mtDNA nt 8993 T→G (ATP6) point mutation associated with Leigh syndrome into mtDNA-less cells demonstrates cosegregation with a decrease in state III respiration and ADP/O ratio. *Proc. Natl. Acad. Sci. U. S. A.* **91**, 8334–8
51. Sgarbi, G., Baracca, A., Lenaz, G., Valentino, L. M., Carelli, V., and Solaini, G. (2006) Inefficient coupling between proton transport and ATP synthesis may be the pathogenic mechanism for NARP and Leigh syndrome resulting from the T8993G mutation in mtDNA. *Biochem. J.* **395**, 493–500
52. Boyer, P. D. (1997) The ATP synthase—a splendid molecular machine. *Annu. Rev. Biochem.* **66**, 717–49
53. Cortés-Hernández, P., Vázquez-Memije, M. E., and García, J. J. (2007) ATP6 homoplasmic mutations inhibit and destabilize the human F₁F₀-ATP synthase without preventing enzyme assembly and oligomerization. *J. Biol. Chem.* **282**, 1051–1058
54. Morava, E., Rodenberg, R., Hol, F., Vries, de M., Janssen, A., Heuvel, L., Nijtmans, L., and Smeitink, J. (2007) Clinical and Biochemical Characteristics in Patients With a High

- Mutant Load of the Mitochondrial T8993G/C Mutations. *Am. J. Med. Genet. A.* **143A**, 2106–2112
55. Debray, F. G., Lambert, M., Lortie, A., Vanasse, M., and Mitchell, G. A. (2007) Long-term outcome of leigh syndrome caused by the NARP-T8993C mtDNA mutation. *Am. J. Med. Genet. Part A.* **143**, 2046–2051
56. Wallace, D. C. (2005) A mitochondrial paradigm of metabolic and degenerative diseases, aging, and cancer: a dawn for evolutionary medicine. *Annu. Rev. Genet.* **39**, 359–407
57. Dionisi-Vici, C., Seneca, S., Zeviani, M., Fariello, G., Rlmoldi, M., Bertini, E., and De Meirleir, L. (1998) Fulminant Leigh syndrome and sudden unexpected death in a family with the T9176C mutation of the mitochondrial ATPase 6 gene. *J. Inherit. Metab. Dis.* **21**, 2–8
58. Jonckheere, A. I., Hogeveen, M., Nijtmans, L. G. J., van den Brand, M. a M., Janssen, A. J. M., Diepstra, J. H. S., van den Brandt, F. C. A., van den Heuvel, L. P., Hol, F. a, Hofste, T. G. J., Kapusta, L., Dillmann, U., Shamdeen, M. G., Smeitink, J. A. M., and Rodenburg, R. J. T. (2008) A novel mitochondrial *ATP8* gene mutation in a patient with apical hypertrophic cardiomyopathy and neuropathy. *J. Med. Genet.* **45**, 129–33
59. Ware, S. M., El-Hassan, N., Kahler, S. G., Zhang, Q., Ma, Y.-W., Miller, E., Wong, B., Spicer, R. L., Craigen, W. J., Kozel, B. a, Grange, D. K., and Wong, L.-J. (2009) Infantile cardiomyopathy caused by a mutation in the overlapping region of mitochondrial ATPase 6 and 8 genes. *J. Med. Genet.* **46**, 308–14
60. De Meirleir, L., Seneca, S., Lissens, W., De Clercq, I., Eyskens, F., Gerlo, E., Smet, J., and Van Coster, R. (2004) Respiratory chain complex V deficiency due to a mutation in the assembly gene *ATP12*. *J. Med. Genet.* **41**, 120–4

61. Wang, Z. G., White, P. S., and Ackerman, S. H. (2001) Atp11p and Atp12p are Assembly Factors for the F₁-ATPase in Human Mitochondria. *J. Biol. Chem.* **276**, 30773–30778
62. Meulemans, A., Seneca, S., Pribyl, T., Smet, J., Alderweirdt, V., Waeytens, A., Lissens, W., Van Coster, R., De Meirleir, L., Di Rago, J. P., Gatti, D. L., and Ackerman, S. H. (2010) Defining the pathogenesis of the human Atp12p W94R mutation using a *Saccharomyces cerevisiae* yeast model. *J. Biol. Chem.* **285**, 4099–4109
63. Honzík, T., Tesarová, M., Mayr, J. a, Hansíková, H., Jesina, P., Bodamer, O., Koch, J., Magner, M., Freisinger, P., Huemer, M., Kostková, O., van Coster, R., Kmoch, S., Houstek, J., Sperl, W., and Zeman, J. (2010) Mitochondrial encephalocardiomyopathy with early neonatal onset due to *TMEM70* mutation. *Arch. Dis. Child.* **95**, 296–301
64. Spiegel, R., Khayat, M., Shalev, S. a, Horovitz, Y., Mandel, H., Hershkovitz, E., Barghuti, F., Shaag, A., Saada, A., Korman, S. H., Elpeleg, O., and Yatsiv, I. (2011) *TMEM70* mutations are a common cause of nuclear encoded ATP synthase assembly defect: further delineation of a new syndrome. *J. Med. Genet.* **48**, 177–82
65. Shchelochkov, O. A., Li, F. Y., Wang, J., Zhan, H., Towbin, J. A., Jefferies, J. L., Wong, L. J., and Scaglia, F. (2010) Milder clinical course of Type IV 3-methylglutaconic aciduria due to a novel mutation in *TMEM70*. *Mol. Genet. Metab.* **101**, 282–285
66. Cízková, A., Stránecký, V., Mayr, J. A., Tesarová, M., Havlíčková, V., Paul, J., Ivánek, R., Kuss, A. W., Hansíková, H., Kaplanová, V., Vrbacký, M., Hartmannová, H., Nosková, L., Honzík, T., Drahot, Z., Magner, M., Hejzlarová, K., Sperl, W., Zeman, J., Houstek, J., and Kmoch, S. (2008) *TMEM70* mutations cause isolated ATP synthase deficiency and neonatal mitochondrial encephalocardiomyopathy. *Nat. Genet.* **40**, 1288–90
67. Mayr, J. A., Havlíčková, V., Zimmermann, F., Magler, I., Kaplanová, V., Ješina, P.,

- Pecinová, A., Nůsková, H., Koch, J., Sperl, W., and Houštěk, J. (2010) Mitochondrial ATP synthase deficiency due to a mutation in the ATP5E gene for the F₁ ε subunit. *Hum. Mol. Genet.* **19**, 3430–3439
68. Tetaud, E., Godard, F., Giraud, M.-F., Ackerman, S. H., and di Rago, J.-P. (2014) The depletion of F₁ subunit ε in yeast leads to an uncoupled respiratory phenotype that is rescued by mutations in the proton-translocating subunits of F_o. *Mol. Biol. Cell.* **25**, 791–9
69. Cipriano, D. J., and Dunn, S. D. (2006) The role of the ε subunit in the Escherichia coli ATP synthase: The C-terminal domain is required for efficient energy coupling. *J. Biol. Chem.* **281**, 501–507
70. Faye, G., Kujawa, C., and Fukushara, H. (1974) Physical and Genetic Organization of Petite and Grade Yeast Mitochondrial DNA 1V. In vivo Transcription Products of Mitochondrial DNA and Localization of 23 S Ribosomal RNA in Petite Mutants of Saccharomyces cerevisiae. *J. Mol. Biol.* **88**, 185–203
71. Lowry, O., Rosebrough, N., Farr, L., and Randall, R. (1951) Protein Measurement with the Folin Phenol Reagent. *J. Biol. Chem.* **193**, 265–275
72. Penefsky, H. S., and Warner, R. C. (1965) Partial Resolution Oxidative of the Enzymes Phosphorylation Catalyzing Oxidative Phosphorylation. *J. Biol. Chem.* **240**, 4694–4702
73. Ito, H., Fukuda, Y., Murata, K., and Kimura, A. (1983) Transformation of intact yeast cells treated with alkali cations. *J. Bacteriol.* **153**, 163–168
74. Walker, J. E., Saraste, M., Runswick, M., and Gay, N. J. (1982) Distantly related sequences in the α and β subunits of ATP synthase, myosin, kinases and other ATP-requiring enzymes and a common nucleotide binding fold. *EMBO J.* **1**, 945–951
75. Blum, D. J., Ko, Y. H., and Pedersen, P. L. (2012) Mitochondrial ATP synthase catalytic

- mechanism: A novel visual comparative structural approach emphasizes pivotal roles for Mg^{2+} and P-loop residues in making ATP. *Biochemistry*. **51**, 1532–1546
76. Hsu, S. Y., Noumi, T., Takeyama, M., Maeda, M., Ishibashi, S., and Futai, M. (1987) Beta-Subunit of Escherichia coli F₁-ATPase. An amino acid replacement within a conserved sequence (G-X-X-X-X-G-K-T/S) of nucleotide-binding proteins. *FEBS Lett.* **218**, 222–226
77. Shen, H., Yao, B. Y., and Mueller, D. M. (1994) Primary structural constraints of P-loop of mitochondrial F₁-ATPase from yeast. *J. Biol. Chem.* **269**, 9424–9428
78. Liang, Y., and Ackerman, S. H. (1996) Characterization of mutations in the β subunit of the mitochondrial F₁-ATPase that produce defects in enzyme catalysis and assembly. *J. Biol. Chem.* **271**, 26522–26528
79. Symersky, J., Osowski, D., Walters, D. E., and Mueller, D. M. (2012) Oligomycin frames a common drug-binding site in the ATP synthase. *Proc. Natl. Acad. Sci. U. S. A.* **109**, 13961–5
80. Ackerman, S. H., and Tzagoloff, A. (2007) Methods to determine the status of mitochondrial ATP synthase assembly. *Methods Mol. Biol.* **372**, 363–77
81. Mukhopadhyay, A., Uh, M., and Mueller, D. M. (1994) Level of ATP synthase activity required for yeast *Saccharomyces cerevisiae* to grow on glycerol media. *FEBS Lett.* **343**, 160–164
82. DeLano, W. L. (2002) The PyMOL Molecular Graphics System, Version 1.1. *Schrödinger LLC*. 10.1038/hr.2014.17
83. Dreusicke, D., and Schulz, G. E. (1988) The switch between two conformations of adenylate kinase. *J. Mol. Biol.* **203**, 1021–1028

84. Saraste, M., Sibbald, P. R., and Wittinghofer, A. (1990) The P-loop - a common motif in ATP- and GTP-binding proteins. *Trends Biochem. Sci.* **15**, 430–434
85. al-Karadaghi, S., Aevarsson, a, Garber, M., Zheltonosova, J., and Liljas, (1996) The structure of elongation factor G in complex with GDP: conformational flexibility and nucleotide exchange. *Structure.* **4**, 555–565
86. Moran, N. A. (1996) Accelerated evolution and Muller's ratchet in endosymbiotic bacteria. *Proc. Natl. Acad. Sci. U. S. A.* **93**, 2873–2878
87. Maisnier-Patin, S., Roth, J. R., Fredriksson, A., Nyström, T., Berg, O. G., and Andersson, D. I. (2005) Genomic buffering mitigates the effects of deleterious mutations in bacteria. *Nat. Genet.* **37**, 1376–1379
88. Fares, M. a, Ruiz-González, M. X., Moya, A., Elena, S. F., and Barrio, E. (2002) Endosymbiotic bacteria: groEL buffers against deleterious mutations. *Nature.* **417**, 398
89. Adachi, H., Katsuno, M., Minamiyama, M., Sang, C., Pagoulatos, G., Angelidis, C., Kusakabe, M., Yoshiki, A., Kobayashi, Y., Doyu, M., and Sobue, G. (2003) Heat shock protein 70 chaperone overexpression ameliorates phenotypes of the spinal and bulbar muscular atrophy transgenic mouse model by reducing nuclear-localized mutant androgen receptor protein. *J. Neurosci.* **23**, 2203–2211
90. White, M., and Ackerman, S. H. (1995) Bacterial production and characterization of ATP11, a yeast protein required for mitochondrial F₁-ATPase assembly. *Arch. Biochem. Biophys.* **319**, 299–304
91. Wang, Z. G., and Ackerman, S. H. (1996) Identification of functional domains in Atp11p: Protein required for assembly of the mitochondrial F₁-ATPase in yeast. *J. Biol. Chem.* **271**, 4887–4894

92. Hinton, A., Zuiderweg, E. R. P., and Ackerman, S. H. (2003) A Purified Subfragment of Yeast Atp11p Retains Full Molecular Chaperone Activity. *J. Biol. Chem.* **278**, 34110–34113
93. Ludlam, A., Brunzelle, J., Pribyl, T., Xu, X., Gatti, D. L., and Ackerman, S. H. (2009) Chaperones of F₁-ATPase. *J. Biol. Chem.* **284**, 17138–17146
94. Cheng, J., Randall, A. Z., Sweredoski, M. J., and Baldi, P. (2005) SCRATCH: A protein structure and structural feature prediction server. *Nucleic Acids Res.*
95. Oldfield, C. J., and Dunker, a K. (2014) Intrinsically disordered proteins and intrinsically disordered protein regions. *Annu. Rev. Biochem.* **83**, 553–84
96. Wang, Z., and Ackerman, S. H. (1996) Identification of Functional Domains in Atp11p: Protein required for assembly of the mitochondrial F₁-ATPase in yeast. **271**, 4887–4894
97. Ackerman, S. H., Martin, J., and Tzagoloff, A. (1992) Characterization of ATP11 and detection of the encoded protein in mitochondria of *Saccharomyces cerevisiae*. *J. Biol. Chem.* **267**, 7386–7394
98. Sikorski, R. S., and Hieter, P. (1989) A system of shuttle vectors and yeast host strains designed for efficient manipulation of DNA in *Saccharomyces cerevisiae*. *Genetics.* **122**, 19–27
99. Yoshida, M., Muneyuki, E., and Hisabori, T. (2001) ATP synthase-a marvellous rotary engine of the cell. *Nat. Rev. Mol. Cell Biol.* **2**, 669–77

ABSTRACT**INVESTIGATION OF MUTATIONS IN NUCLEAR GENES THAT AFFECT THE ATP SYNTHASE**

by

RUSSELL L. D'SOUZA**August 2016****Advisor:** Dr. Sharon Ackerman**Major:** Biochemistry and Molecular Biology**Degree:** Doctor of Philosophy

The F₁ domain is the catalytic subunit of the mitochondrial ATP synthase. Studies with respiratory-deficient yeast identified *ATP1* and *ATP2* as nuclear genes encoding the alpha and beta subunits, respectively, of the mitochondrial F₁-ATPase. The mutations in the *atp1* and *atp2* genes were cloned and sequenced, and they appear to affect the ATP synthase. Most yeast strains with mutations in the β or the α subunit primarily show an F₁ assembly defective phenotype. This feature is similar to the assembly-defective mutants missing the chaperones required for assembly of the F₁ oligomer or either the alpha/beta subunits.

Some of the *atp2* and *atp1* yeast mutants are interesting because they show evidence of a soluble F₁ oligomer with "new" phenotypic characteristics. The yeast strains E892 and E793 with a mutation in the P-loop are capable of assembling the F₁ in vivo, but extraction of the F₁F_o from the inner mitochondrial membrane using detergent renders it unstable forming oligomeric structures. The yeast mutant E323 has a phenotypic characteristic that resembles F₁ assembly defective mutants. However, the defect is not because the mutation affects the structural stability of the protein but due to the inability of the $\alpha\beta$ dimers to assemble a soluble F₁. The yeast mutant

N15 presents two mutations (G227D, D469N) in the beta subunit with impaired catalytic activity. Work in our lab has shown that *atp2* yeast mutants with the G227D mutation are incapable of assembling the F₁F_o. We suggest that the D469N mutation rescues the deleterious phenotypic effect of the G227D mutation.

The F₁- α and β subunits are assembled into a soluble hexamer with the aid of two nuclear-encoded chaperones Atp12p and Atp11p respectively. Chaperones maintain the activity of proteins that are destabilized by mutations. Prokaryotes show increased levels of chaperones to alleviate the deleterious effects of mutations. To explore this possibility, we overexpressed the *ATP11* and *ATP12* genes to determine if it rescues the mutant phenotype. Our efforts so far have proved unsuccessful.

Thus, to summarize, we biochemically evaluated the effect of mutations in the *atp1* and *atp2* genes of the F₁-ATPase. The work presented here will give valuable insight into the role of individual amino acids in the functioning of the ATP synthase. Mutational studies combined with structural data will allow us to completely understand the mechanism of the ATP synthase.

AUTOBIOGRAPHICAL STATEMENT

Russell L. D'Souza

Russell D'Souza graduated with a Bachelor's of Science in Chemistry from St. Xavier's College, Mumbai. He then obtained a Master's degree in Biotechnology from YCM University, Nasik. During his Master's degree he was involved in a project that looked at delivering the drug Doxycycline using nanoparticles. On completion of his Master's degree, he secured a position as a Research Associate in the drug metabolism and pharmacokinetics department, at Piramal Life Sciences Ltd. During this time, he looked at the role of P-glycoprotein that is involved in the efflux of various small molecules from the intestine using the Caco2 cell culture system. This work has led to the publication of two manuscripts which Russell D'Souza has co-authored. Furthermore, he also investigated enzyme induction and inhibition of Cytochromes P450, a liver enzyme, using microsomal fractions and cell culture assays. Following this, he applied to the USA for graduate studies and was accepted for a doctoral program in the Department of Biochemistry and Molecular Biology, at Wayne State University, School of Medicine. He entered the laboratory of Dr. Sharon Ackerman as a rotational student and decided to continue graduate studies in her lab. As part of his research project, he has investigated the role of mutations in the *ATP1* and *ATP2* genes of the mitochondrial F₁-ATP Synthase. Separately, he has also performed studies on the *ATP11* and *ATP12* genes, that are assembly factors that aid in the biogenesis of the mitochondrial F₁F₀ as a complete oligomer.